Organisms Diversity & Evolution (2020) 20:681–699
https://doi.org/10.1007/s13127-020-00459-8

ORIGINAL ARTICLE

How to build a larval body with less than a hundred cells? Insights from the early development of a stalked jellyfish (Staurozoa, Cnidaria)

Tatiana D. Mayorova[1,2] · Boris Osadchenko[3] · Yulia Kraus[2,3]

Received: 8 April 2020 / Accepted: 1 September 2020 / Published online: 1 October 2020

Abstract
The stalked jellyfish (Staurozoa) is an extraordinary clade within medusozoan cnidarians in which the medusa is attached to the substrate unlike the pelagic jellyfishes which compose the rest of the medusozoans. Along with this remarkable feature, staurozoans are characterized by an extremely low number of cells (< 100) in the embryos and larvae. The aim of the present study is to explore early development of the staurozoan *Lucernaria quadricornis* and to elucidate morphogenetic events evolved to overcome the constraints imposed by low cell number. Using bright field, confocal, and electron microscopy, we create a normal table of development of *Lucernaria*, describe cell number dynamics, and visualize organization of embryos and larvae. From these data, we infer a crosstalk between cell reshaping, cell rearrangement, and mechanical stress, involved in gastrulation, anterior-posterior axis differentiation, and even locomotion of the larva. Our work also demonstrates that staurozoans convergently developed morphogenetic pathways similar to other very distant animals with low cell number in the early development. We consider *Lucernaria* as an EvoDevo model with potential for further research to answer the question of how evolutionary forces act on developmental trajectories.

Keywords Cnidaria · Gastrulation · Morphogenesis · Cell reshaping · Cell rearrangement · Body axis differentiation

Introduction

"There are still very little data on the development of the genus *Lucernaria*" ("Über die Entwicklungsgeschichte der Lucernarien besitzen wir noch wenige Angaben"). This is the first sentence of a paper written by Alexander Kowalevsky in 1884, and this is still true, despite the attempts to fill the gap in the knowledge on the development of *Lucernaria* and other staurozoan cnidarians (Bergh 1888; Hanaoka 1934; Kowalevsky 1884; Otto 1976; Wietrzykowski 1910, 1912). Are there any objective reasons for embryologists to re-investigate early development of these animals?

Early development can change in many different ways during evolution; surprisingly, developmental trajectories can vary dramatically within the same phylum, for example variation in the segmentation of short germband and long germband insects (Clark 2017; Lynch et al. 2012); variation in the cleavage and gastrulation in vertebrates/mollusks having big yolky eggs (teleost fishes/cephalopods) and small yolk-poor eggs (mammals/some gastropods) (Hejnol 2010; Ivanova-Kazas 1995; Kalinka and Tomancak 2012). This leads to an interesting conundrum of highly plastic early developmental stages underlying robust body plans (Raff 1992; Wray and Raff 1991). It appears that changes in early development caused by adaptive evolution of life-history traits (maternal investment, rate of development, etc.) are only possible in association with the compensatory changes in developmental trajectory providing the robust formation of the adult body plan. The intriguing question is how these evolutionary processes interact. To approach this question, we need versatile and tractable model organisms demonstrating clear examples

✉ Tatiana D. Mayorova
mayorova@wsbs-msu.ru

✉ Yulia Kraus
yulia_kraus@mail.ru

[1] Laboratory of Neurobiology, National Institute of Neurological Disorders and Stroke, National Institutes of Health, 49 Convent Drive, Bethesda, MD 20892, USA

[2] Koltzov Institute of Developmental Biology of Russian Academy of Sciences, Vavilova 26, Moscow 119334, Russia

[3] Faculty of Biology, Lomonosov Moscow State University, Leninskiye gory 1/12, Moscow 119234, Russia

of directed changes in developmental trajectory occurring over the course of evolution. We define the "developmental trajectory" as potentially variable and evolvable chain of developmental events (Burggren and Reyna 2011; Smith et al. 2015). We use this notion to emphasize that we focus on the developmental processes rather than on the set of discrete stages.

One type of the developmental trajectories, not widely spread but represented in different groups of bilaterian animals, is associated with the dramatic reduction of cell number at early developmental stages. Early embryos of some nematodes, spiralians (e.g., Rotifera, Gastrotricha, Sipuncula, some gastropod mollusks), and chordates (Tunicata) are characterized by a small number of cells (Hejnol 2010; Schierenberg 2001; Schulze and Schierenberg 2011). In spite of the fact that the embryogenesis of at least some of these animals was described in high detail, it has never been inferred how exactly low cell number influences morphogenetic pathways in these embryos, and if these animals have any common developmental traits which might be a direct consequence of a low cell number.

Furthermore, low cell number is observed in non-bilaterian animals as well, for example in the poor studied early development of the cnidarian *Lucernaria* (Bergh 1888; Hanaoka 1934; Kowalevsky 1884; Otto 1976; Wietrzykowski 1910, 1912). In the phylum Cnidaria, evolutionary simple body plan is coupled with a high level of evolutionary and developmental plasticity. Cnidarians deploy a wide range of developmental trajectories, and their complex life cycle has been subjected to multiple evolutionary modifications (Boero et al. 1992; Leclère et al. 2016). *Lucernaria* belongs to the class Staurozoa (stalked jellyfishes) within the medusozoan cnidarians (Collins et al. 2006; Miranda et al. 2016). In contrast to other medusozoans (Hydrozoa, Scyphozoa, and Cubozoa), staurozoans never produce free-swimming medusae, and their sedentary adult stage combines both medusa and polypoid features (Miranda et al. 2016). Staurozoans spawn several thousand tiny eggs (25–50 μm) at once, and their embryos and larvae consist of extremely few cells (< 100) (Kowalevsky 1884; Otto 1976). By contrast, many other cnidarian species consist of about 10,000 cells at the late embryonic and larval stages (Plickert et al. 1988; Yuan et al. 2008). Such a low number of cells indicates that severe constraints are imposed on all developmental processes and staurozoans have had to modify developmental trajectory to overcome these constraints. That is why we consider the staurozoan representatives as very promising models for EvoDevo. A thorough study of their development is essential to gain a deeper insight into the evolutionary forces acting on developmental trajectories and complex life cycles of metazoans.

Here, we report a comprehensive study of embryonic and larval development of the staurozoan *Lucernaria quadricornis* (O. F. Müller, 1776). We create a table of *Lucernaria* development and describe peculiar morphogenetic events, which allow the embryo to overcome the developmental constraints imposed by a low number of cells. We show that an extremely high blastomere to embryo volume ratio results in an increased morphogenetic role of each individual cell. Moreover, we identify specific morphogenetic events uniting nearly all few cell embryos described so far (including *Lucernaria*), which we consider are the pathways to overcome the aforementioned constraints.

Material and methods

Animal culture

Sexually mature stauromedusae were collected in August of 2015, 2016, and 2017 at the Moscow State University Pertsov White Sea Biological Station (WSBS MSU) (Kandalaksha Bay, White Sea, Russia, 66° 34′ N, 33° 08′ E) by SCUBA diving. Collected animals were kept in jars at 8 °C and were fed newly hatched *Artemia salina* nauplii once a day. Once the animals spawned spontaneously, the eggs were transferred to Petri dishes with filtered seawater and kept at 8 °C during all further development.

In vivo observations

The embryos were imaged every 4–5 h using a light microscope (Leica DM2500; Leica Microsystems, Wetzlar, Germany) with a built-in 10MP digital camera.

Fluorescent labeling and confocal microscopy

Embryos and larvae were fixed in freshly prepared 4% paraformaldehyde (Fluka, Germany) in 0.1 M phosphate-buffered saline (PBS, pH 7.4; Fluka, Germany) overnight at 4 °C. From body elongation onwards, all individuals were relaxed by adding 0.7 M $MgCl_2$ prior to fixation. After permeabilization with 0.1% Triton X-100 (Ferak Berlin, Germany) in PBS (PBST), the samples were incubated in anti-acetylated alpha-tubulin mouse antibody diluted 1:2000 (Sigma, USA) in PBST at 4 °C for 24 h. After rinsing with PBST, a mixture of Alexa 647 conjugated goat anti-mouse antibody (1:500; Molecular Probes, USA), phallacidin-bodipy (1:200; Thermo Fisher Scientific, USA), and propidium iodide (10 μg/mL; Sigma-Aldrich, MO, USA) or DAPI (1 μg/mL; Molecular Probes, USA) in PBST was applied at room temperature for 3–4 h. After washing in PBS, the samples were cleared in increasing grades of glycerol/PBS and mounted in 70% glycerol.

Images were collected with a 63× objective at 60–120 nm/px resolution on a Nikon A1 CLSM (Nikon Instruments, Japan). Image stacks of optical sections were scanned with a

1-μm step size. Acquired z-stacks were exported to ImageJ 2.0.0 (NIH, USA) to make maximum intensity projections and adjust brightness and contrast.

Cell counts were performed for each development stage in at least five specimens using ImageJ software. Nuclear dyes did not label the nuclei before the end of gastrulation. Hence, the number of cells was counted based on phallacidin staining only; both phallacidin and nuclear staining was used for cell counts at post-gastrulation stages.

Transmission electron microscopy

Transmission electron microscopy (TEM) was performed as described previously (Burmistrova et al. 2018). Since the embryos clump together, they were processed in small groups, which greatly facilitated handling of such tiny embryos. Planulae were processed individually and cut longitudinally.

Results

We herein describe stage-by-stage early development of *Lucernaria*, with emphasis on morphogenetic events that underlie normal development.

Staging

We used in vivo observation to characterize main developmental stages and to create a table of development.

Lucernaria egg is about 40 μm in diameter (Fig. 1a). The reliable sign of fertilization was separation of the fertilization membrane from the surface of an egg which could be detected during about an hour after spawning. We designated this event as the initial point and registered time of development from that moment. A zygote underwent holoblastic equal cleavage. The cleavage was synchronous for all blastomeres during the first four divisions, which took place every 5 h and resulted in a 16-cell blastula with no cavity inside (Fig. 1b–e). The embryo cleaved then asynchronously. Gastrulation began at approximately 25 hpf, when the presumptive endoderm cells elongated along the apico-basal axis (Fig. 1f). Elongated blastomeres deepened inside the embryo (Fig. 1g), and gastrulation resulted in a solid gastrula. Both ectoderm and endoderm were easily distinguished at the late gastrula stage (Fig. 1h). The morphological differentiation of anterior–posterior (AP) axis began after 40 hpf. Endoderm changed its shape gradually inside the still spherical embryo (it took 15–20 h): it became ellipsoidal first (Fig. 1i, j), and in the process of further elongation, it curled up (Fig. 1k). At the next step, the embryo body as a whole elongated along the AP axis: The forming larva (about 60 hpf) was curled inside the fertilization membrane (Fig. 1l). Planula hatched from fertilization membrane on the third day of development. The hatching planula unfolded the body leaving the fertilization membrane (Fig. 1m) and crawled slowly by bending the body. Hatchlings measured about 85 μm in length and 30 μm in diameter. The larva increased its length soon after the hatching, so its body was about 120 μm in length and still about 30 μm in diameter (Fig. 1n).

Thus, we suggest the following key stages of *Lucernaria* early development: cleavage, gastrulation, morphological differentiation of the AP axis, and planula. We then investigated each of these stages in detail using confocal and electron microscopy.

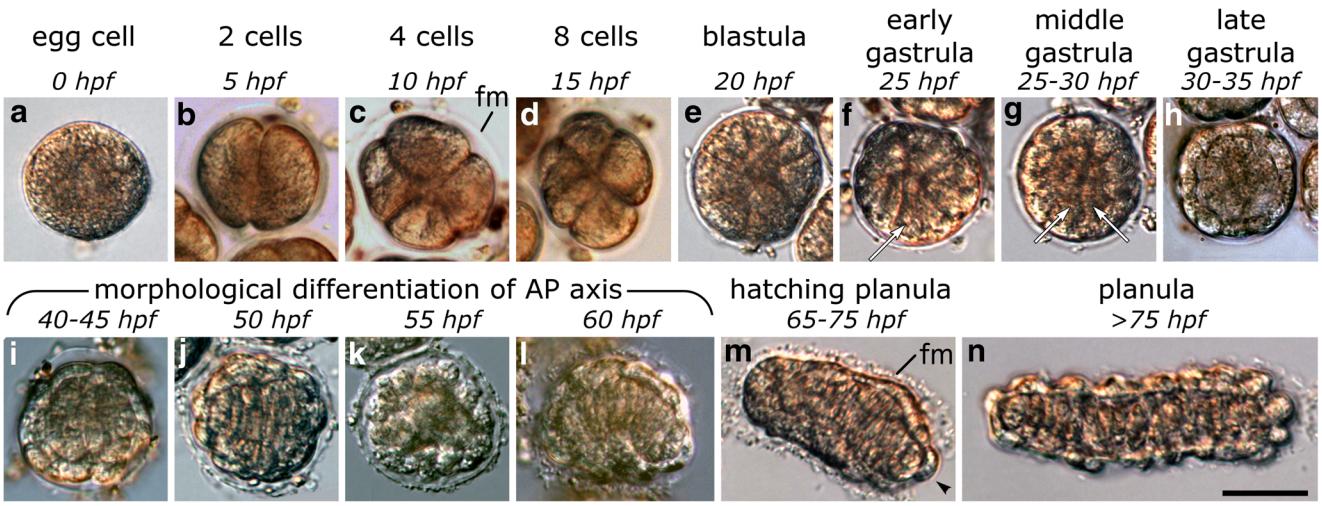

Fig. 1 Timing of the development of *Lucernaria* embryo up to the planula larva stage: in vivo light microscopy imaging. The time of development at +8 °C is given in hours post fertilization (hpf). Note that neither embryo nor planula have cavity. The name of developmental stage is indicated on the top of each image. White arrows on (**f**) and (**g**) point at the cells moving inside the embryo during gastrulation (the gastrulation pole is down). The primary body (AP) axis is horizontal on (**i**)–(**n**). Black arrowhead on (**m**) points to the rupture of the fertilization membrane that appears right before hatching. fm, fertilization membrane. Scale bar: 30 μm

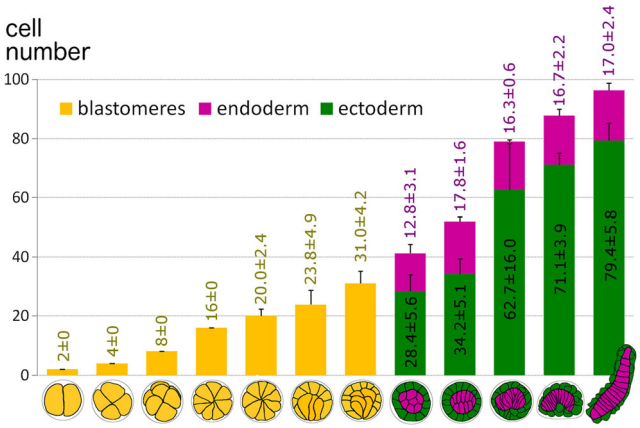

Fig. 2 Dynamics of cell number during early development of *Lucernaria*. Mean ± St. dev

Cleavage and blastula stage

We did not fix the embryos at a stage of synchronous cleavage because they were too fragile, and their organization and cell number could be easily assessed in living embryos (see previous discussion).

The number of blastomeres ranged from 18 to 23 in a blastula when the cells began to divide asynchronously (after 16-cell stage, Fig. 2). All the blastomeres were of the same size (Fig. 3a) and had a cone-like shape with narrow part directed inside the embryo (Fig. 3b). Both confocal and electron microscopy confirmed that blastula had no cavity inside, and so it can be called "stereoblastula" (Fig. 3b, c). The content of the blastomeres was highly heterogeneous and included multiple electron-dense yolk granules (1–2 μm) and vacuoles (from 200 nm to 2 μm), which were evenly distributed throughout the cytoplasm excluding the perinuclear area (Fig. 3c, d). Characteristic electron-dense cortical granules of the uniform size about 400 nm were found right beneath the apical membrane (Fig. 3d, e). The apical membrane of blastomeres had scarce microvilli (Fig. 3e). The blastomeres were tightly packed and demonstrated an extensive area of septate junctions (Fig. 3f).

Gastrulation

The number of cells in the embryos at the beginning of gastrulation was highly variable (from 16 to 28, Fig. 2). In fact, some embryos started to gastrulate as early as at the 16-cell stage, that is right after the fourth synchronous division.

The first sign of gastrulation was that 2–4 cells at the presumably animal pole of the embryo became columnar, while the rest of the blastomeres retained their wedge-like shape (Fig. 4a). The apical part of the elongated cells then began to narrow, and their basal portion became enlarged, so these cells acquired characteristic bottle shape (Fig. 4a′, b, c) associated with the gastrulation by ingression (e.g., Shook and Keller 2003). The apical membrane of bottle cells had multiple folds (Fig. 4c, d). The adjacent ectoderm cells stretched out their edges towards the site of ingression, so their shape on a section was triangular (Fig. 4a′, b). The ectoderm cells on the side opposite to gastrulation site were trapezoidal.

The number of cells increased moderately as gastrulation proceeded and averaged 31 at the middle gastrula stage (Fig. 2). At this stage, reshaping of both ecto- and endoderm cells became more dramatic. The apical surface of ingressing cells shrank to a minute width (Fig. 4a″, e–g), and some of these cells already submerged inside the embryo (Fig. 4a‴, e). Phallacidin staining was very intensive in the apices of the ingressing cells (Fig. 4a″, a‴). The cells of presumptive ectoderm located near the ingression site protruded their edges and formed thin lamellae covering presumptive endoderm cells (Fig. 4f, g).

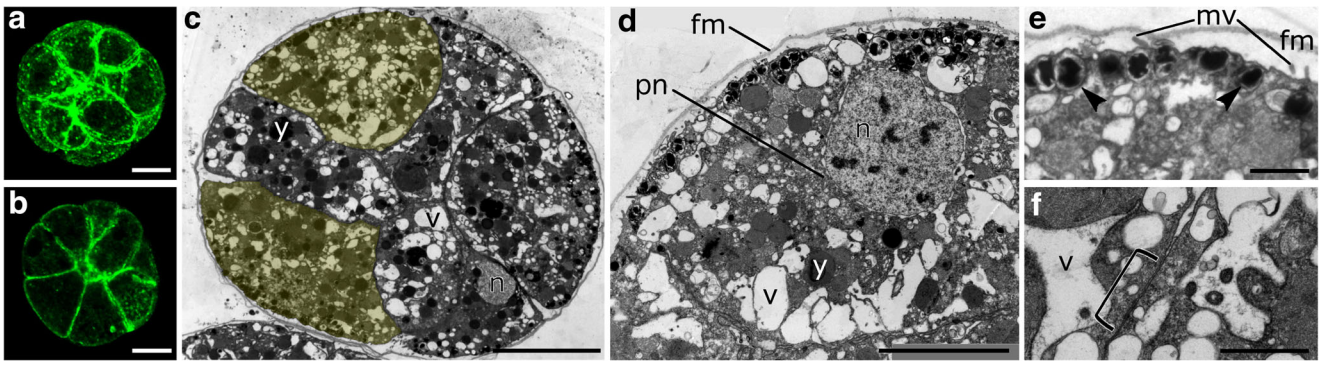

Fig. 3 Stereoblastula: CLSM of phallacidin staining (**a**, **b**) and TEM (**c**–**f**). (**a**) A 16-cell stage embryo, maximum intensity projection; cell cortices are labeled with phallacidin (green). (**b**) Central optical section through the stereoblastula: all blastomeres are roughly of the same size and shape. (**c**) Section through the center of an embryo showing that there is no blastocoel inside the blastula. Two blastomeres are artificially colored in yellow. (**d**) A blastomere has multiple yolk granules and vacuoles; the perinuclear cytoplasm is free of yolk granules. (**e**) apical cortical area of a blastomere with electron-dense granules (black arrowheads). The apical surface bears microvilli. (**f**) Septate junction (bracket) between the adjacent blastomeres. fm, fertilization membrane; mv, microvilli; n, nucleus; pn, perinuclear cytoplasm; v, vacuoles; y, yolk granules. Scale bars: (**a**–**c**) 10 μm; (**d**) 5 μm; (**e**, **f**) 1 μm

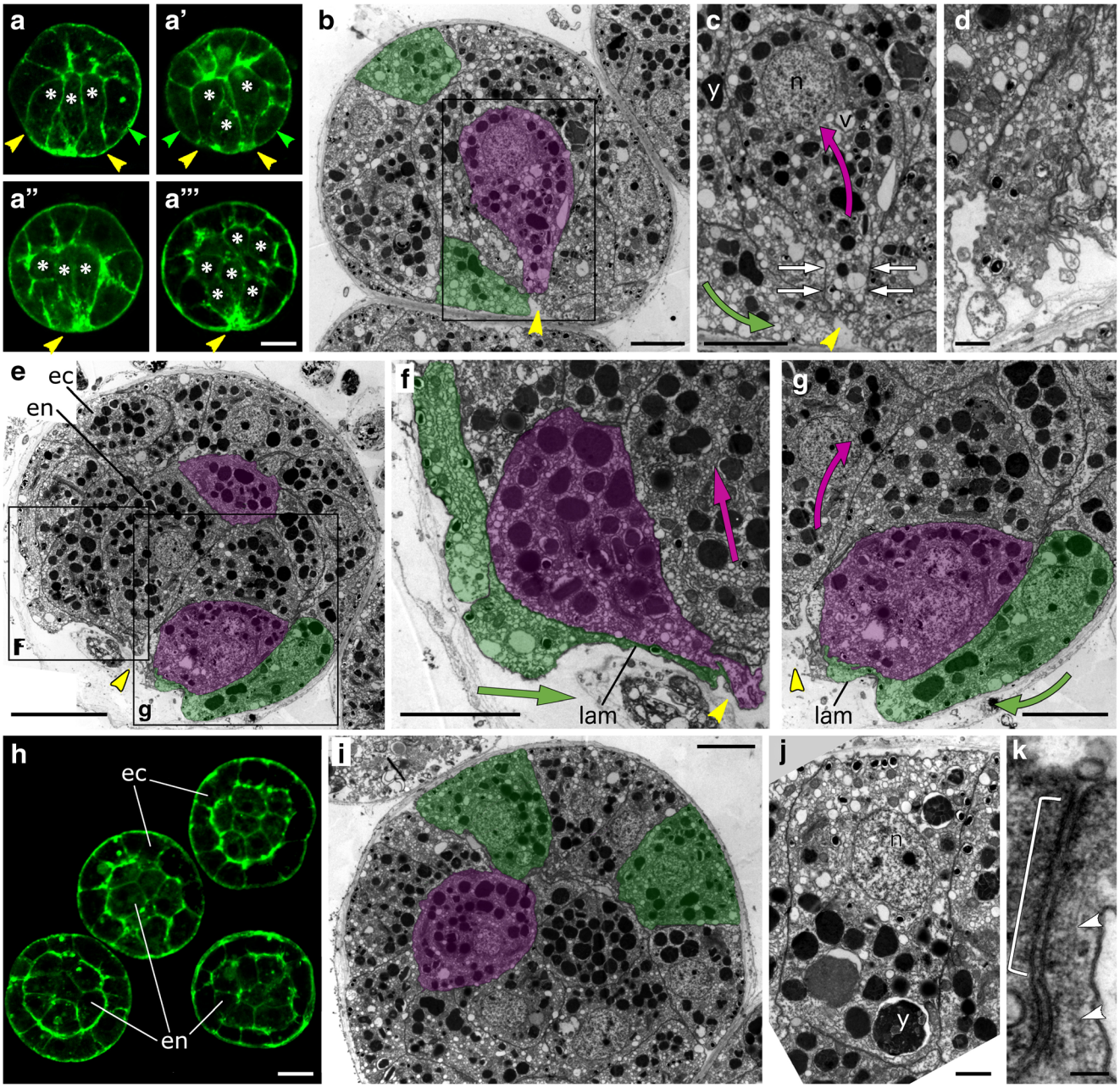

Fig. 4 The dynamics of gastrulation: CLSM of phallacidin staining (**a**, **h**) and TEM (**b**–**g**, **i**–**k**). Embryos are oriented with the gastrulation pole (yellow arrowheads) down. Prospective ectoderm cells are artificially colored in green and prospective endoderm cells are artificially colored in purple on the TEM images. (**a**–**a‴**) Successive stages of gastrulation, central optical sections. Note the columnarized (**a**) and then bottle-shaped (**a′**–**a‴**) presumptive endoderm cells marked with asterisks and stretching ectoderm cells (green arrowheads) adjacent to the site of ingression. (**b**) An embryo at the early gastrula stage (corresponds to **a′**). Presumptive ectoderm cells situated near the ingressing cells are stretched towards the pole of gastrulation, while the cells beyond this area have a cuboid shape. (**c**) Close-up of the region framed on B showing ultrastructure of an ingressing cell. White arrows demonstrate the constriction of the cell apex. A purple arrow shows the direction of squeezing of the enlarged basal portion of the cell inside the embryo and a green arrow shows the direction of stretching of ectoderm cells. (**d**) Ultrastructure of the constricted apex of an ingressing cell. Note multiple folds on the apical surface. (**e**) The mid-gastrula stage embryo (corresponds to **a‴**). (**f**) and (**g**) Close ups of the areas framed on (**e**). Note bottle and drop shapes of ingressing cells. Flattened ectoderm cells form thin lamellae to cover the site of ingression. Movements of endoderm and ectoderm cells are shown with purple and green arrows, respectively. (**h**) The late gastrula stage, optical section through the center of embryos. (**i**) At the late gastrula stage endoderm cells are rounded, and ectoderm cells are trapezoidal. (**j**) Close up of a trapezoidal ectoderm cell. (**k**) Ectoderm cells are linked to each other by septate junctions (bracket); arrowheads point to the microtubules associated with the junction area. ec, ectoderm; en, endoderm; lam, lamellae; n, nucleus; v, vacuole; y, yolk granule. Scale bars: (**a**–**a‴**, **e**, **h**) 10 μm; (**b**, **c**, **f**, **g**, **i**) 5 μm; (**d**, **j**) 1 μm; (**k**) 100 nm

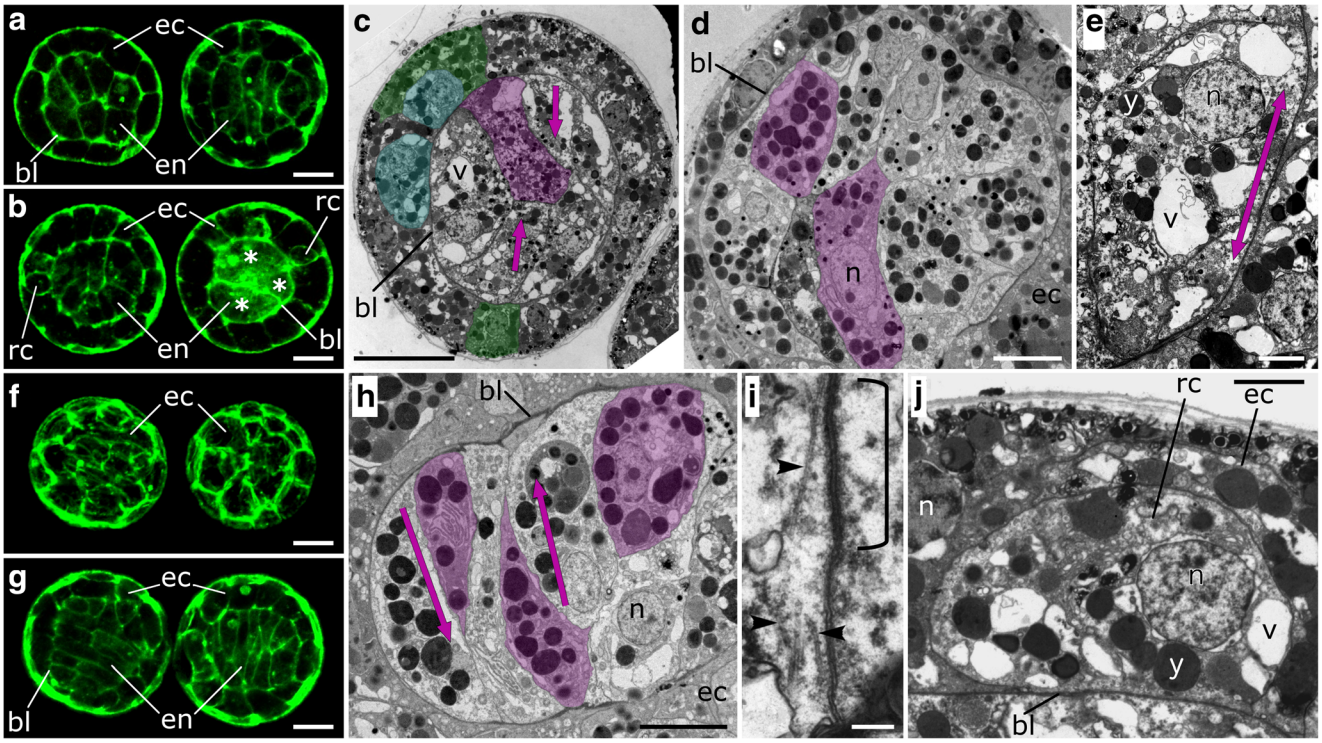

Fig. 5 Morphological differentiation of the AP body axis: beginning of endoderm cell reshaping. CLSM of phallacidin staining (**a**, **b**, **f**, **g**) and TEM (**c**–**e**, **h**–**j**). Ectoderm cells are artificially colored in green (rounded basiepithelial cells are in cyan) and endoderm cell are artificially colored in purple on the TEM images. (**a**–**e**) Primary elongation of endoderm cells. (**a**) Very beginning of the axis development: some endoderm cells start elongating. (**b**) Embryos at a bit later stage: longitudinal section (left) and cross section (right). Endoderm cells are elongated perpendicular to the body axis. As they are packed in two rows, only two or three cells (asterisks) are visible on a cross section. Rounded cells lacking the contact with the embryo surface appear in the ectoderm. (**c**) An embryo at the same stage as on (**b**), longitudinal section. Purple arrows show the direction of elongation of the endoderm cells. Note plenty of vacuoles in their cytoplasm. (**d**) The endoderm core with characteristic pairwise arrangement of cells. (**e**) Ultrastructure of an endoderm cell. A purple double-headed arrow shows the direction of cell elongation. (**f**–**j**) Endoderm cells continue elongating and start to intercalate between each other. (**f**) Maximum intensity projections reconstructing 3D view of the embryos. (**g**) Longitudinal optical section of the embryos on (**f**). Endoderm cells are arranged in pairs (left embryo) and start to intercalate between each other (right embryo). (**h**) Endoderm cell intercalation: the free edges of endoderm cells intercalate between each other and spread (purple arrows) towards the opposite side of the basal lamina. (**i**) Septate junction (bracket) between the neighboring endoderm cells. Arrowheads point to the microtubules associated with the junction area. (**j**) High magnification of a rounded cell occupying the basiepithelial position in the ectoderm. bl, basal lamina; ec, ectoderm; en, endoderm; n, nucleus; rc, round cell; v, vacuole; y, yolk granule. Scale bars: (**a**–**c**, **f**, **g**) 10 μm; (**d**, **h**) 5 μm; (**e**, **j**) 2 μm; (**i**) 200 nm

The overall number of cells increased considerably at the late gastrula stage: it almost doubled since the beginning of gastrulation. The average numbers of ectoderm and endoderm cells were 28 and 13, respectively (Fig. 2). The embryo demonstrated clearly distinguishable ectoderm and endoderm layers (Fig. 4h). Blastomeres were of the same shape and size within each germ layer: ectoderm cells were cuboid or trapezoidal, while cells of endoderm were polygonal or rounded (Fig. 4h–j). There was no apparent difference between the content of ectoderm and endoderm cells: Both of them had round nuclei and plenty of yolk granules and small vacuoles in cytoplasm (Fig. 4i, j). All cells were tightly packed, and the surface of the embryo was even. The apices of ectoderm cells were anchored to each other by septate junctions (Fig. 4k). The diameter of an embryo stayed about 40 μm.

Morphological differentiation of anterio-posterior axis

The first morphological signs of anterio-posterior (AP) axis differentiation appeared when the embryo had 30–40 ectoderm cells and 14–19 endoderm cells (Fig. 2). At this stage, some endoderm cells started to elongate in the direction perpendicular to the future AP axis. They changed their shape from rounded to oval (Fig. 5a). As endoderm cells continued elongation (purple arrows on Fig. 5c and e), they acquired columnar or trapezoidal shape on the sections (Fig. 5b–e). At the same time, they flattened in the plane perpendicular to the plane of elongation. The free edges of elongating cells met each other along the middle line of the endoderm core, and thus endoderm cells became arranged in two rows as appeared on the longitudinal sections (Fig. 5b–d). Therefore,

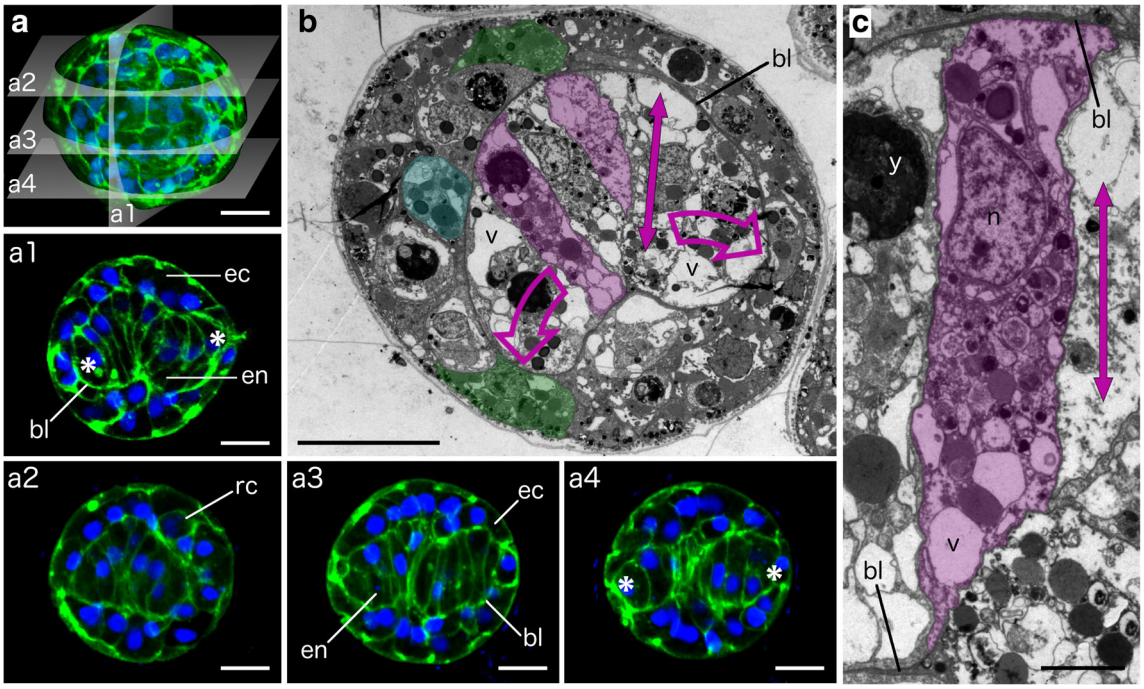

Fig. 6 Morphological differentiation of the primary body axis: development of the endoderm rod. Cell cortices are labeled with phallacidin (green) and nuclei are labeled with DAPI (blue) on the CLSM images (**a**, **a1**–**a4**). Ectoderm cells are artificially colored in green (round cells are in cyan) and endoderm cells are artificially colored in purple on the TEM images (**b**, **c**). Future poles of AP body axis are marked with asterisks. (**a**) 3D reconstruction of a spherical embryo. (**a1**–**a4**) Planes of the longitudinal optical sections. (**a1**) Section of the embryo in the plane of the endoderm rod bending: the endoderm rod of the spherical embryo has a V shape. (**a2**–**a4**) Optical sections through the embryo in the planes perpendicular to the axis of the rod bending, which demonstrate topology of the V-shaped endoderm rod at the different levels; note two separate pieces of endoderm on (**a3**) and (**a4**) representing cross-cuts of "V" branches. (**b**) The endoderm rod curls inside the spherical embryo (hollow purple arrows); a double-headed purple arrow shows the directions of cell intercalation. More than a half of endoderm cells have a contact with the basal lamina on their both sides on the section; therefore, they finalize establishment of the contact with basal lamina throughout the entire perimeter. (**c**) An endoderm cell, both sides of which contact the basal lamina. bl, basal lamina; ec, ectoderm; en, endoderm; n, nucleus; rc, rounded cell; v, vacuole; y, yolk granule. Scale bars: (**a**, **a1**–**a4**, **b**) 10 μm; (**c**) 2 μm

only two or three endoderm cells appeared on the cross-sections (Fig. 5b, right embryo).

Endoderm cells of still spherical embryos (Fig. 5f) kept further elongating and flattening, and eventually the cells from the opposite rows started to intercalate between each other (Fig. 5g, purple arrows on Fig. 5h). The endoderm core became slightly elongated along the AP axis (Fig. 5h). During intercalation, endoderm cells acquired a drop shape on sections: their free edges were getting narrow and spread towards the basal lamina of the opposite side of the core. Despite the fact that endoderm cells moved actively along each other they had extensive areas of septate junctions (Fig. 5i). Their cytoplasm was enriched with microtubule bundles oriented along the cell long axis (Fig. 5i).

At this stage, the first ultrastructural difference became apparent between ecto- and endoderm cells: the last had more vacuoles and their cytoplasm was clearer (Fig. 5c, d, h). Basal lamina separating ecto- and endoderm appeared at this stage (Fig. 5c, d, h).

We found the first sign of cell differentiation in the ectoderm. Most ectoderm cells were still cuboid and demonstrated thick belts of the filamentous actin in the sub-apical cortex (Fig. 5f, g). However, a small group of cells lost the contact with the surface while kept the contact with the basal lamina, submerged into the ectodermal epithelium and rounded up (Fig. 5b, c, j). Their content was similar to that of other ectodermal cells.

The next developmental stage was the last one when the embryo shape was spherical (Fig. 6a) and therefore had the size and shape exactly the same as the egg cell. Endoderm cells continued intercalation and began to form a single row. Finally, this cell rearrangement resulted in the elongation of the endoderm core, thus forming the rod-like structure (further referred to as the "endoderm rod"), which at this stage curled up inside the spherical embryo (Fig. 6a1, B, hollow purple arrows). When we optically cut an embryo in the plane of rod bending, we can view bended V-shaped ectoderm rod (Fig. 6a1). When we cut an embryo in the planes perpendicular to the axis of rod bending, the appearance of the rod depended on the depth of sectioning. Fig. 6a2 shows the section through the base of "V." Figure 6a3 shows the section taken from the middle of "V" and so visualizes two oblique sections of branches of "V." On Fig. 6a4, the V-shaped rod is cut through the tips of "V" branches, corresponding to future poles of AP axis (asterisks).

The sections made in different planes demonstrated that many endoderm cells had already acquired the shape of a disc (or coin) and established contact with the basal lamina throughout the disk periphery (Fig. 6a1–a4, solid purple arrows on B and C). However, a few cells still had free edges squeezed between neighboring endoderm cells (Fig. 6b). The vacuoles of endoderm cells got larger; all together, they occupied a considerable portion of the cell (Fig. 6b, c).

This stage was characterized by two-fold increase in the number of ectoderm cells, while the number of endoderm cells remained unchanged (Fig. 2). In fact, this was the largest increase of ectoderm cell number during early development of *Lucernaria*. Otherwise, the ectoderm layer was not subject to any significant changes since the previous stage: it consisted of cuboid cells and a few rounded cells (Fig. 6a2, B). The surface of the embryo was smooth.

The next development stage finalized endoderm cells rearrangement and resulted in the formation of a bean-shaped embryo elongated along the AP axis; elongation of the whole body was registered for the first time during embryogenesis. The ectoderm added approximately 10 cells at this stage while the number of endoderm cells did not change (Fig. 2). As a rule, one end of an embryo started to protrude from the rounded body (Fig. 7a–d, purple arrow on d). Longitudinal sections showed that the endoderm rod, being curled at a previous stage, straightened out now (Fig. 7b–d). Although all endoderm cells were flattened, their shapes differed from one another as they were still rearranging to form a single row. This accounted for rough surface and overall irregular shape of the endoderm rod (Fig. 7b–d).

Later on, endoderm cells finished their alignment, so when the embryo finally adopted a bean shape (Fig. 7e–g), the endoderm rod was straighter (Fig. 7i, purple arrows on Fig. 7j), and its contour was smooth (Fig. 7f, h–j). Each endoderm cell except for two semi-oval terminal cells acquired coin-like shape, so all of them were attached to the basal lamina around the perimeter (Fig. 7f, h–k). Their nuclei were noticeably flattened to fit inside the narrow cell (Fig. 7j, k). The diameter of the endoderm rod was about 17 μm (Fig. 7f, h, i).

Once the elongation of the body began, the surface of the embryo ceased to be smooth for the first time during the development. This was a result of reshaping of ectoderm cells: the shape of individual cells ranged from flattened to columnar with all variants in between, which directly affected the thickness of the ectoderm (Fig. 7b, white double arrows). Remarkably, the areas of thickened ectoderm even had peculiar festoon-like folds on the surface (Fig. 7b, c, j, l). These folds appeared as protrusions of cell apices, which seemed to rise up above the level of belted subapical septate junctions (Fig. 7m). By contrast, other areas of ectoderm were so thin, that it looked like the endoderm rod was exposed to the environment (Fig. 7b, c, f, i). In fact, the ectoderm layer in these areas was represented by lamellae of ectoderm cells, measuring less than 1 μm in thickness (Fig. 7j, n). Typically, the areas of thinned ectodermal epithelium were found on the tips of an embryo as well as in the middle of the body (Fig. 7f, i). Rounded cells looking similar to that described before were still present in the ectoderm (Fig. 7d, j, inset on n).

Fig. 7 Morphological differentiation of AP axis: elongation of the body along AP axis and rearrangement of ectoderm cells. Cell cortices are labeled with phallacidin (green) and nuclei are labeled with DAPI (blue) on the CLSM images (**a**–**c**, **e**–**i**). Asterisks mark the poles of AP axis. Ectoderm cells are artificially colored in green (rounded cells are in cyan) and endoderm cells are artificially colored in purple on the TEM images (**d**, **j**–**n**). (**a**) Maximal intensity projection reconstructing 3D view of an embryo: one pole of the body axis (outlined with dashed line) protrudes from the spherical part of the embryo. (**b**) Single section of the embryo shown on (**a**). Double-headed arrows emphasize the ectoderm thickness in the different regions of the embryo. Note that ectoderm cells are concentrated in a spherical part of the embryo, and form festoon-like folds (white arrowheads), while the outgrowth is covered with very few flattened ectoderm cells (red arrowhead). (**c**) Single section of another embryo at the same stage exemplifying irregular shaped endoderm rod and unevenly distributed ectoderm cells. (**d**) The endoderm rod: an outgrowth forms at one side of the embryo (purple arrow). Almost all endoderm cells have their both sides contacting the basal lamina. (**e**–**i**) CLSM images of bean-shaped embryos. (**e**, **g**) 3D reconstructions of bean-shaped embryos. (**f**, **h**) optical sections of the embryos shown on (**e**) and (**g**), respectively; final stage of intercalation: All endoderm cells contact the basal lamina by their both sides (**h**). Note the areas with extremely thin ectoderm (red arrowheads on (**f**)). (**i**) An optical section from the convex side of bean-shaped embryo. Note precise alignment of cells of the endoderm rod. (**j**) Longitudinal section of an embryo finalizing intercalation of endoderm cells. The endoderm rod unfolds (purple arrows) along the AP axis pulling the ectoderm sheet (green arrows) to cover its poles. The ectoderm has several folds (white arrowheads). (**k**) Endoderm cell with both short sides contacting the basal lamina. (**l**) Festoon-like fold (white arrowhead) between apices of two adjacent ectoderm cells. Arrow points at the contact between two cells. (**m**) Intercellular junction (bracket) between two ectoderm cells. (**n**) Close up of the region framed on (**j**). Extremely thin edge of the ectoderm cell covers one of the ends of the endoderm rod. Inset shows rounded basiepithelial ectoderm cell. bl, basal lamina; ec, ectoderm; en, endoderm; n, nucleus; rc, round cell; v, vacuole. Scale bars: (**a**–**j**) 10 μm; (**k**, **l**, **n**, inset on **n**) 2 μm; (**m**) 200 nm

Hatchlings and planulae

During hatching, an embryo ruptured the fertilization membrane and escaped to the environment. From this time point we considered it as a planula larva. The body of hatching planula reached the length of 100 μm (Fig. 8a, b). All endoderm cells were perfectly aligned so the rod surface was "seamless" and smooth. The meshwork of vacuoles which seemed to fuse was visible in the endoderm cells (Fig. 8a, c). The planula body was straight or slightly curved.

The body surface was bumpy; many ectoderm cells were stretched or overlapped one another (Fig. 8a). The apical membrane was densely covered with microvilli (Fig. 8a, c, d). The ectodermal rounded cells, the content of which did not differ from other ectoderm cells before hatching, now

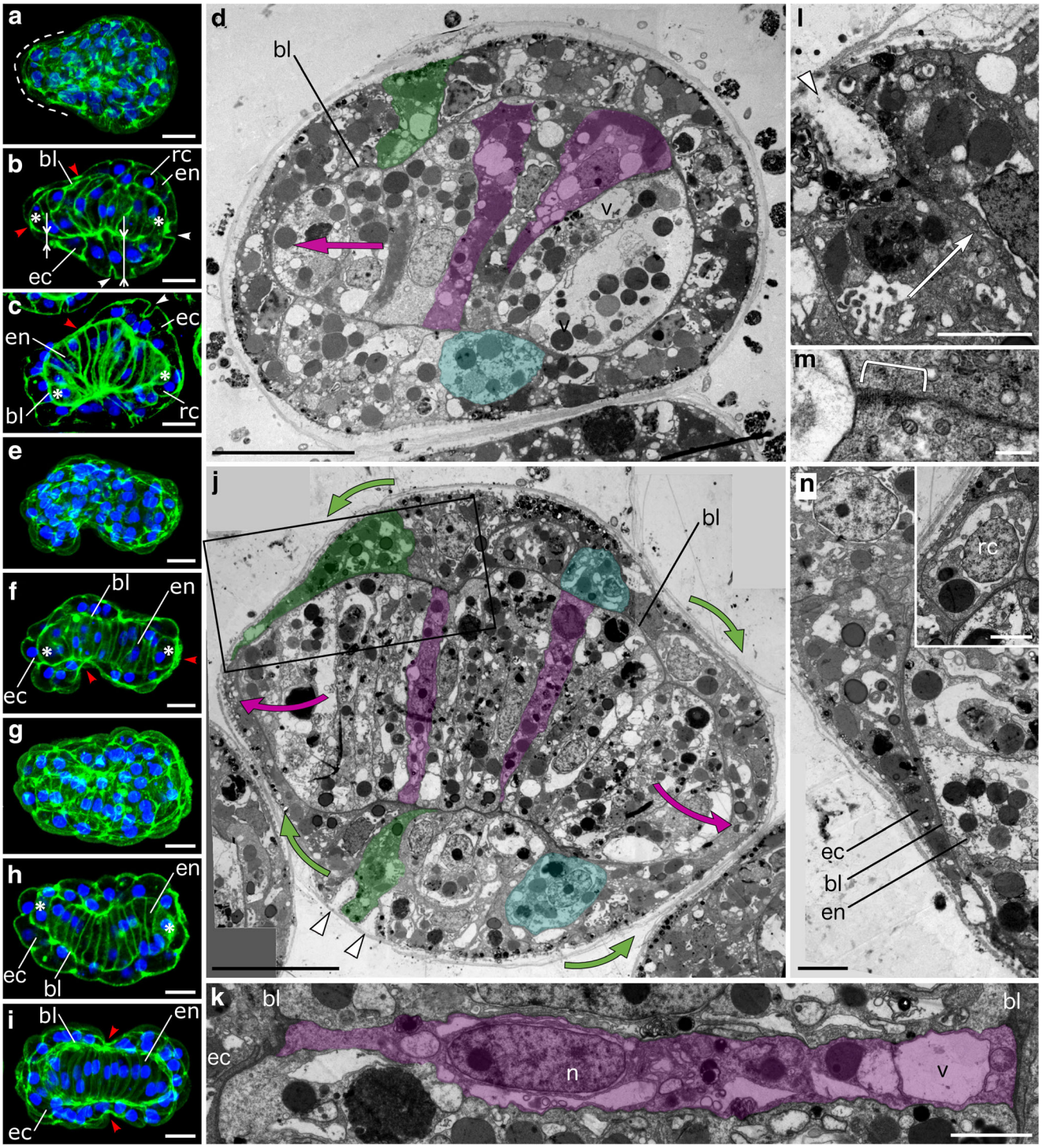

demonstrated a small 2.5 × 1 μm capsule characteristic of a cnidoblast cell (Fig. 8a, d, e). The cnidoblast capsules were also detected with anti-acetylated α-tubulin antibodies (Fig. 8b). At this stage, when the body was straight enough, it became apparent that these cells occupied the area equal to about one third of body length near one pole. Each hatchling had 3–7 cnidoblasts. Thus, the poles of a planula were morphologically different. We also noticed that phallacidin staining along the basal lamina was more intensive in the part of hatchlings lacking cnidoblasts (Fig. 8b).

Planulae older than one day after hatching differed from hatchlings. Most of them had 75–85 ectoderm cells and 16 or 18 cells within the endoderm rod; however, the number of endoderm cells ranged from 14 to 23 cells (Fig. 2, Fig. 9a–c). Planulae crawled in a worm-like manner, i.e., by bending and contracting the body. Multiple processes of myoepithelial cells

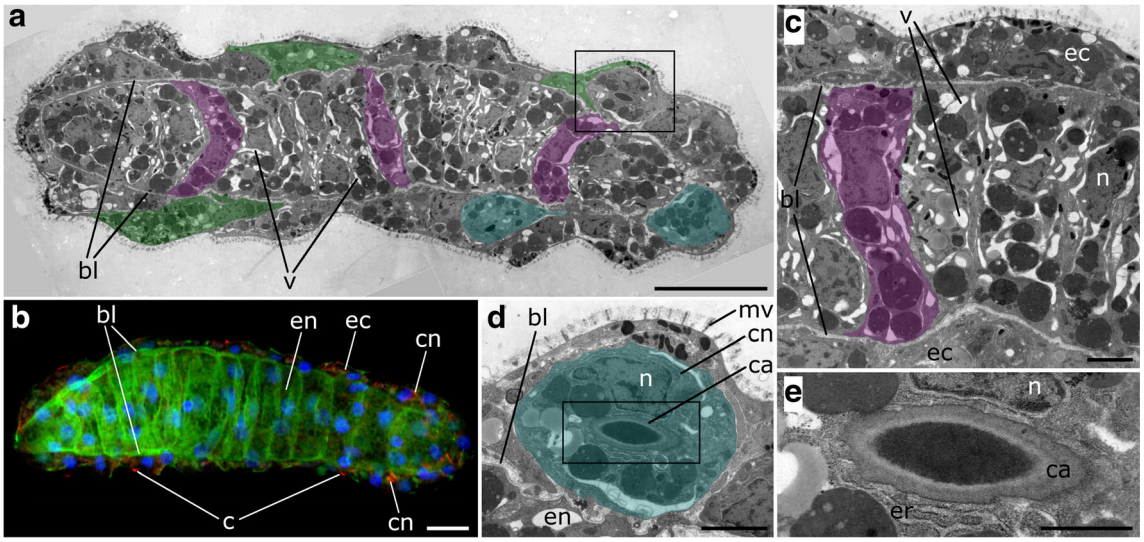

Fig. 8 Hatchling stage. Cell cortices and myonemes are labeled with phallacidin (green), nuclei are labeled with DAPI (blue), cilia and cnidoblasts are labeled with anti-tubulin antibodies (red) on the CLSM image (**b**). Ectoderm cells are artificially colored in green (cnidoblasts are cyan) and endoderm cells are artificially colored in purple on the TEM images (**a**, **c**–**e**). The pole of the hatchlings with cnidoblasts is oriented to the right. (**a**, **b**) Longitudinal sections through the body axis. The endoderm rod straightens, endoderm cells are coin-shaped, and ectoderm cells are of irregular shape. Sparse cilia are observed for the first time at this stage. Cnidoblasts are located at one pole of the hatchling body. (**c**) Higher magnification of the middle part of the hatchling body. Endoderm cells contain large number of vacuoles. (**d**) Close up of the region framed on (**a**) showing a cnidoblast sitting on the basal lamina and covered with neighboring cells on the top. (**e**) Higher magnification of the differentiating cnidoblast framed on (**d**). *bl*, basal lamina; *c*, cilium; *ca*, capsule; *cn*, cnidoblast; *ec*, ectoderm; *en*, endoderm; *er*, endoplasmic reticulum; *mv*, microvilli; *n*, nucleus; *v*, vacuole. Scale bars: (**a**, **b**) 10 μm; (**c**, **d**) 2 μm; (**e**) 1 μm

enabling worm-like movements of planula were visualized in the area of the basal lamina (Fig. 9d). The processes of myoepithelial cells running along and around the body were organized into the muscular network (Fig. 9d, inset). As in hatchlings, muscular network had much more intense phallacidin staining in that half of a planula lacking cnidoblasts (Fig. 9e, f). Intriguingly, we noticed that the shape of planula cells changed dynamically as the planula contracted its body. Contracted regions of planula body were characterized by a bumpy surface of ectoderm cells, relatively thick ectoderm, and narrowed endoderm cells (Fig. 9e, f). By contrast, smooth ectoderm surface, thin ectoderm, and wide endoderm cells characterized relaxed regions (Fig. 9e, f). Though ectoderm cells changed their shape and overlapped each other, they were still anchored to one another by subapical septate junctions (Fig. 9g).

Planulae strikingly increased the body length to up to 150 μm (Fig. 9a–c) which is 1.5 times more than in hatchlings; the increase of length was likely a result of significant widening of the endoderm cells (Fig. 9a–c). They were almost completely filled with a large vacuole (Fig. 9a, b) that was electron transparent on the TEM images (Fig. 9c, h, i). The vacuole occupied all central parts of each cell leaving islands of cytoplasm between itself and the plasma membrane (Fig. 9c, h, i). As a result, the nucleus was located eccentrically (Fig. 9i). Two terminal endoderm cells were semi-oval or cone-shaped and did not demonstrate any difference between each other at an ultrastructural level (Fig. 9j, k). As before, the larvae had no gastric cavity.

Fig. 9 Planula larva stage, three days after hatching. Cell cortices and myonemes are labeled with phallacidin (green), nuclei are labeled with DAPI (blue), cilia and cnidoblasts are labeled with anti-tubulin antibodies (red) on the CLSM images (**a**, **b**, **d**–**f**, **l**, **n**). Ectoderm cells are artificially colored in green (cnidoblasts are cyan) and endoderm cells are artificially colored in purple on the TEM images (**c**, **g**–**k**, **m**, **o**). The pole of the planula with cnidoblasts is oriented to the right. (**a**, **b**) The larvae with very low (14 on **a**) or very high (23 on **b**) number of endoderm cells. (**c**) Longitudinal section. Note large vacuoles in the endoderm cells. (**d**) Maximum intensity projection of two tangential optical sections showing longitudinal and circular myonemes. Inset is a close up of the framed region. (**e**, **f**) The shape of both ectoderm and endoderm cells reflects the locomotor activity of the planula. White lines render the contour of ectoderm and outline individual endoderm cells. (**g**) Septate junction (bracket) between ectoderm cells. (**h**) A middle part of the planula body. (**i**) Higher magnification of an endoderm cell. The large single vacuole, occupying the center of the cell, swells and increases the volume of the cell (purple arrows). (**j**) The pole with no cnidoblasts. The ectoderm cell protrusions hardly cover the tip of the endoderm rod. (**k**) The pole with cnidoblasts at different stages of differentiation. (**l**) A planula with 16 endoderm cells and well developed cnidoblasts. (**l′** and **l″**) Other examples of the cnidoblast pole. (**m**) Ultrastructure of a cnidoblast. Large capsule has twisted thread inside, while the rest of the forming thread is yet outside the capsule. (**n**) Tangential optical section through the ectoderm surface showing that each epithelial ectoderm cell bears one cilium. (**n′**) Superficial view on three ectoderm cells. (**n″**) Side view shows that cilia lie on the cytoplasmic membrane. (**o**, **o′**) Serial sections of a cilium. Note how tight a cilium is to the cytoplasmic membrane. bb, basal body; bl, basal lamina; c, cilium; ca, capsule; ce, centriole; cn, cnidoblast; ec, ectoderm; en, endoderm; mv, microvilli; n, nucleus; r, rootlet; th, thread; v, vacuole. Scale bars: (**a**, **b**, **d**–**f**, **l**, **n**) 20 μm; (**c**) 10 μm; (**h**, **j**, **k**, insets on **d**, **l**, **n**) 5 μm; (**i**, **m**) 2 μm; (**g**, **o**, **o′**) 200 nm

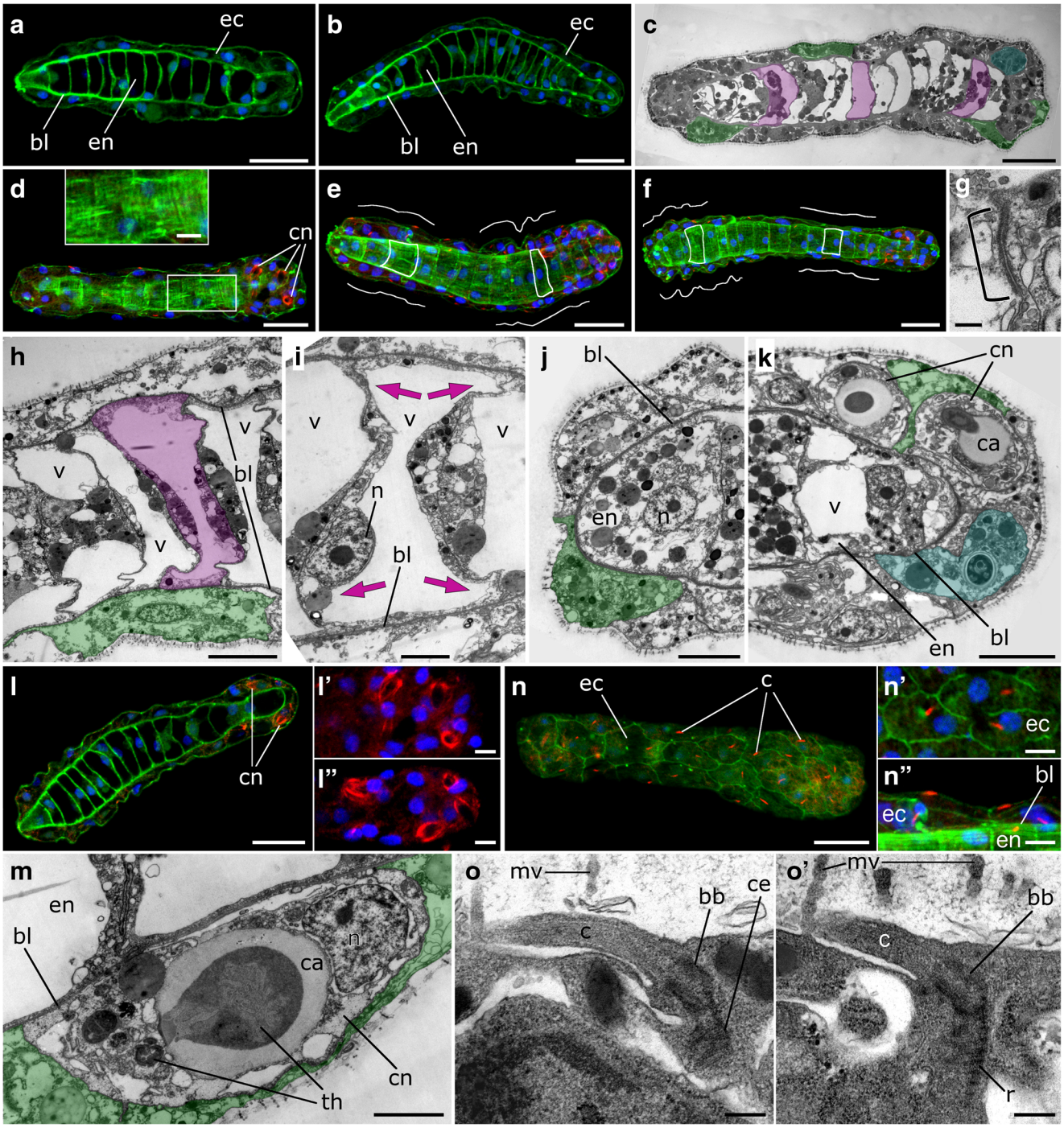

The two poles of larva could not be distinguished in living animals. They both dynamically changed the shape from thin and conical to enlarged and blunt. However, studying the ultrastructure, we noticed that the ectoderm sheet was much thinner at the pole lacking cnidoblasts (Fig. 9j). Under light microscopy, it looked like the terminal endoderm cell was exposed to the environment (Fig. 9a, b, l). Nevertheless, it was covered by thin edges of ectoderm cells meeting each other at the very tip of the planula (Fig. 9j). Apparently, the most obvious difference between the two poles of *Lucernaria* larva was the presence of cnidoblasts in the ectoderm of one pole (Fig. 9c, k). The cnidoblasts retained their location being attached to the basal lamina and covered with ectoderm cells on top. Capsules inside cnidoblasts were outlined by anti-tubulin staining (Fig. 9d, l, l′, l″), probably associated with supportive rods of the capsule (Raikova 1990; Rifkin and Endean 1988). In comparison with the hatchling stage when tiny lentil shape capsules measured only one micron, the capsules of older planula were round or oval with 5–6 μm diameter and occupied a considerable part of a cnidoblast (Fig.

9k, m). In some cnidoblasts, the thread was not completely packed inside the capsule, and we could identify the thread parts as an electron-dense material in the cytoplasm (Fig. 9m).

Despite the fact that planulae moved by muscular contractions only, they developed short cilia detected with anti-acetylated alpha-tubulin antibodies. The first sparse cilia were registered at the hatchling stage (Fig. 8b); they increased their number and length over a few next days after hatching. Basically, each epithelial ectoderm cell had one cilium (Fig. 9n, n′). Thus, the superficial cells of *Lucernaria* planula are monociliated. The cilia were extremely short, not longer than 4 μm. Instead of being upright, they followed the contour of the cell (Fig. 9n″). EM studies confirmed that cilia adhered tightly to the cell membrane and never protruded above the level of microvilli (Fig. 9o, o′) In most cases, a cilium was directed towards the pole with no cnidoblasts. We also revealed a basal body, an accessory centriole (Fig. 9o) and striated ciliary rootlet (Fig. 9o′).

Discussion

Morphogenic movements in metazoans are based on the force-generating activity of multiple individual cells integrated into "morphogenic machines" (Shook et al. 2018; Shook and Keller 2008). How can we detect these "morphogenic machines" in the development of certain species? More than 50 years ago, Jane Westfall pointed out: "The morphologist is usually confronted with the challenging task of illuminating a dynamic process of development or function from a series of static pictures" (Westfall 1966). However, recent studies showed that a series of cell shape changes might tell us an amazingly complete story about the morphogenetic activity of this cell (Blankenship et al. 2006; Haas et al. 2018; Kraus et al. 2014; Lecuit and Lenne 2007; Sawyer et al. 2010). Based on the detailed description of embryonic cells in *Lucernaria,* we further suggest the main "morphogenic machines" operating in the embryo consisting of only few cells.

Small number of cells determines the mode and mechanics of gastrulation

The initial conditions for gastrulation are created in the process of cleavage. In *Lucernaria*, cleavage (Fig. 1b–d, Fig. 10a–c) results in stereoblastula, which consists of ~20 wedge-shaped epithelial cells (Fig. 1e, Fig. 3b, c, Fig. 10d). Thus, the initial conditions, which apparently affect the mechanics of gastrulation, are low number of cells, absence of blastocoel and large cell size in relation to size of an embryo. In all staurozoans studied in this respect, small embryo size was associated with very few cells (Kowalevsky 1884; Otto 1976; Wietrzykowski 1912).

In many animals, apical constriction of bottle cells has been considered as one of the major forces driving gastrulation (Sawyer et al. 2010). Morphologically, bottle cells of *Lucernaria* (Fig. 4a′, b, c) are similar to those found in gastrulating embryos of other cnidarians (Byrum 2001; Kraus and Technau 2006) and bilaterians (Shook and Keller 2003). The difference lies in the cell behavior. Ingressing cells normally move far away from the site of gastrulation crawling over the blastocoel roof (Byrum 2001; Momose and Schmid 2006). In *Lucernaria*, ingressing cells have no room to crawl. Instead, they get inside the embryo only by changing the shape. Initially, wedge cells (Figs. 3b, 10d) change their shapes to columnar (Figs. 4a, 10e), and then, through the bottle-like forms and drop-like forms with almost reduced apices (Figs. 4a′–a‴, 10e, f), to the rounded ones (Figs. 4h, 10g). Constriction of cell apices (Fig. 4c, d) is provoked most likely by contraction of actomyosin meshwork (Roh-Johnson et al. 2012), that is reflected by an intensive phallacidin staining of the apical F-actin (Fig. 4a″, a‴). This constriction results in inward displacement of much of the intracellular contents (Fig. 4c, f, g, purple arrows). Thus, reshaping of the cell causes its inward displacement without its actual movement.

It is important that the constriction of cell apices generates physical forces on the embryo surface, which stretch the remaining surface cells. Vectors of these forces are directed towards the ingression site. The presumptive ectoderm cells have to expand their apices to restore the mechanical equilibrium: they change their shapes from wedge-like to trapezoidal (compare the shapes on Fig. 4a–a‴). This, in turn, gives the ingressing cells the room to sink inside and, at the same time, provides an additional surface to cover the site of ingression. At the mid-gastrula stage, the ectoderm cells adjacent to the ingression site form long lamellae, which help to seal the hole left in the epithelium (Fig. 4f, g, green arrows). This cell behavior is evolutionary conserved and can be found in EMTs of many animals (Shook and Keller 2003).

Taken together, gastrulation of *Lucernaria* combines very special types of ingression and epiboly as an elegant solution to the problem of low cell number. Other staurozoans described manifest the same way of cleavage and gastrulation (Hanaoka 1934; Otto 1976; Wietrzykowski 1912).

Morphological differentiation of the primary body axis: endoderm cell rearrangement, development of the endoderm rod

The embryos of *Lucernaria* begin morphological differentiation of AP axis once the endoderm cells reach the final quantity registered in planula, typically 16 or 18 (Fig. 2). The same was observed in another staurozoan, *Halyclistus* (Wietrzykowski 1912).

Planar cell intercalation is a widespread morphogenetic movement leading to elongation of epithelium in the direction

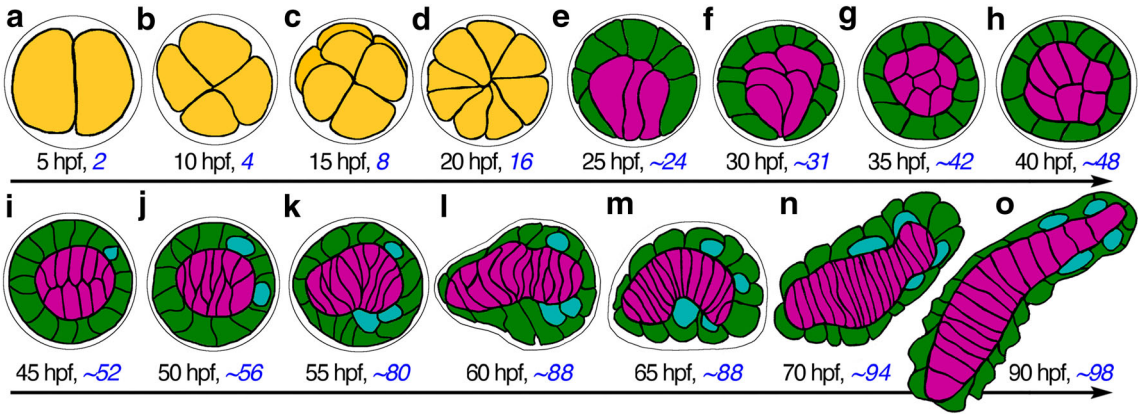

Fig. 10 Schematic representation of embryonic and larval development of *Lucernaria*. Blastomeres are yellow, ectoderm cells are green (cnidoblasts are cyan) and endoderm cells are purple. Cell number is indicated in blue font. (**a**–**c**) Cleavage. (**d**) Stereoblastula. (**e**, **f**, **g**) Early, mid-, and late gastrulae, respectively. (**h**, **i**) Beginning of morphological differentiation of the AP body axis: the endoderm cells elongate perpendicular to the future AP axis. (**j**) Beginning of intercalation of endoderm cells. (**k**) Endoderm rod develops as an outcome of endoderm cell intercalation and curls up inside the spherical embryo. (**l**) Endoderm rod straightening, beginning of ectoderm cells rearrangement and elongation of the body axis. (**m**) Endoderm cells complete intercalation at the stage of a bean-shaped embryo. (**n**) straightening of the body axis and hatching. (**o**) Elongated planula larva with highly vacuolated swelled endoderm cells, a few days after hatching

perpendicular to cell movement. For example, mediolateral cell intercalation during gastrulation and neurulation underlies body plan establishment in vertebrate embryos (Keller et al. 2000). It also plays an essential role in the AP axis development in embryogenesis of invertebrates, for example, in hydrozoan cnidarians (Kraus 2006; Kraus et al. 2014) and in the nematode *Caenorhabditis elegans* (Priess and Hirsh 1986; Simske and Hardin 2001). In these embryos, ectoderm cells play a leading role in embryo lengthening along the AP axis. *Lucernaria* embryo is a remarkable exception in that AP elongation is initiated by intercalation of not ectoderm, but endoderm cells (Figs. 5h, 6b, 7b–d, 10h–m).

Typically, cell intercalation proceeds by changing neighbors that leads to planar translocation of epithelial cell (Keller et al. 2000). Because of the tight packing of cells in a minute and solid *Lucernaria* embryo, endoderm cells do not have enough room to change *location*; instead, they only change *the shape* to finally form a rod of aligned cells.

Rounded/polygonal endoderm cells flattens on one axis to form a coin-like shape (Figs. 10g–m, 11) establishing the contact with the basal lamina throughout whole perimeter of the "coin." The intercalation and alignment of the endoderm cells (Fig. 11d) ultimately leads to elongation of the endoderm rod (Fig. 11e). Initially, the rod curls inside the spherical ectoderm sheath, which serves as a physical boundary limiting the length and shape of the rod. Once intercalation is complete, the rod is becoming straight and eventually straightens the entire body of a prehatching embryo (Fig. 11f).

Taken together, the endoderm cells undergo sophisticated 3-D reshaping, which can be considered a driving force of AP elongation of *Lucernaria* embryo.

Morphological differentiation of the primary body axis: ectoderm rearrangement, elongation of the body axis

The ectoderm epithelium remains morphologically unchanged throughout endoderm rod formation (Figs. 5, 6). However, there is a significant peak in proliferative activity at the stage of endoderm rod formation (Fig. 2). Apparently, the ectoderm epithelium is a mechanically integral structure, as evidenced from septate junctions between adjacent cells (Figs. 4k, 5i, 7m) enforced by microfilament bundles (Fig. 5a, b, f, g). We hypothesize that strong mechanical stress imposed by the elongating and curling endoderm rod on ectoderm sheet is what triggers mitosis in ectoderm cells (Gudipaty et al. 2017; Liu et al. 1993). The doubling of ectoderm cells number is essential for covering the endoderm rod, the surface area of which has been increased significantly during its reshaping from rounded to elongated form.

Elongation of endoderm certainly leads to rearrangement of ectoderm cells. Diversity of cell shapes (Fig. 7j), different thickness of ectoderm sheet (Fig. 7b), extremely thin cell protrusions (Fig. 7n), and festoon-like folds (Fig. 7j, l) are evidence for the ectoderm being under mechanical stress and active rearrangements (Clark et al. 2014; Salbreux et al. 2012). As cells have the tendency to move in that way to compensate for mechanical stresses (Beloussov 1996), they redistribute on the endoderm rod surface (Fig. 7j, green arrows). From this point, ectoderm does not restrain the endoderm; instead, it follows the shape of the rod, and the embryo body becomes elongated (Figs. 7h, i, 10l, m).

Therefore, mechanical stresses imposed by the endoderm rod formation induce changes in the ectoderm cell behavior, crucial for the transformation of a spherical

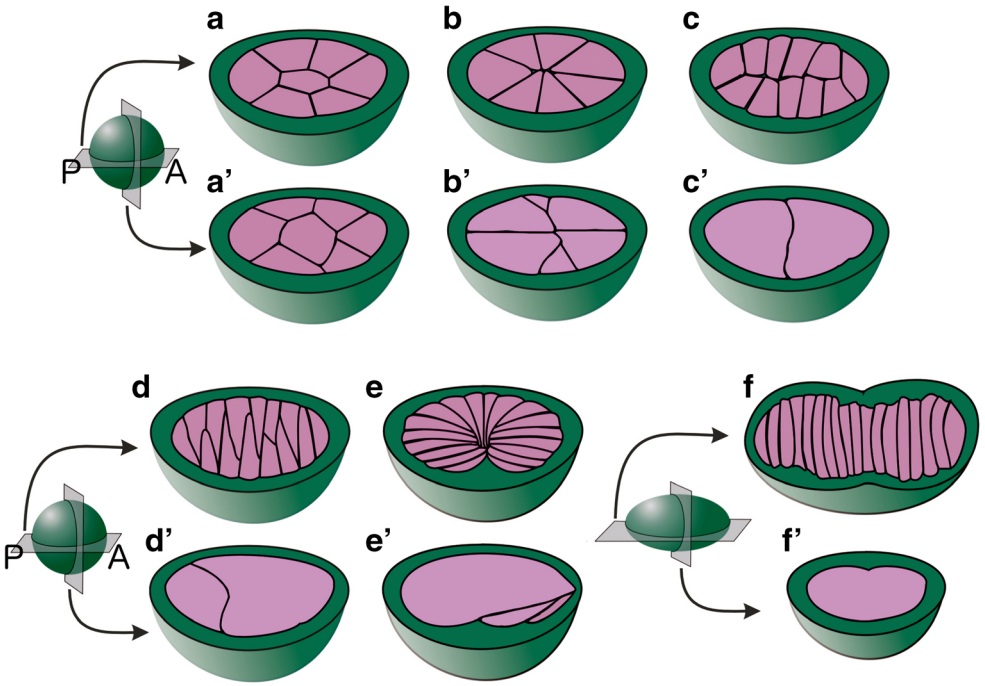

Fig. 11 Schematic drawing depicting rearrangement and reshaping of endoderm cells during AP axis development seen from two mutually perpendicular planes. Upper row (**a**–**f**) represents a cut along the AP axis; lower row (**a′**–**f′**) represents a cut perpendicular to the AP axis. Ectoderm is green, endoderm cells are purple. After gastrulation (**a**, **a′**), endoderm cells acquire a two-row organization by getting polarized perpendicular to the AP axis (**b, b′, c, c′**). Later on, the opposite cells intercalate between each other (**d, d′**) resulting in the elongation and curling of the endodermal core (**e, e′**), which finally forces the whole body of the larva to elongate (**f, f′**). At this stage, all endoderm cells are lined up in a single cell row (**f, f′**)

embryo into a worm-like planula, the next developmental stage of *Lucernaria*.

Planula of *Lucernaria*: "hairless worm" in an otherwise ciliated world of cnidarians?

The endoderm cells differ from the ectoderm cells by the high content of small and medium sized vacuoles; this difference becomes already visible in the beginning of AP axis differentiation (Fig. 5c, d). When a planula hatches, the vacuoles in the endoderm cells increase their size (Fig. 8c) probably by fusing with one another. Then, when the larva spends a while in seawater, the vacuoles expand dramatically (Fig. 9h, i, purple arrows) increasing the length of the endoderm rod and, therefore, the whole planula body (Fig. 10n, o). Most likely, the rod elongates by the same mechanism as the notochord of amphibians and fish, where vacuoles swell osmotically (Adams et al. 1990; Thomas and Stemple 2004). Swelling of endoderm cell is a mechanism, by which hatched larvae not only increase their length, but also obtain hydrostatic skeleton probably contributing to their movement.

Staurozoan planula crawls on the substrate making vermiform moves (Kowalevsky 1884; Otto 1976) provided by contractions of longitudinal and circumferential processes of myoepithelial cells (Fig. 9d). Since cells and body are comparable in size due to low cell number, all changes in planula body shape (bending, stretching, etc.) induce deformation of individual cells, both ectoderm and endoderm (Fig. 9e, f).

Since the time of first discovery of weird looking staurozoan larvae, it has been considered that these planulae lack cilia, and that is why they crawl instead of swim (Hanaoka 1934; Kowalevsky 1884; Otto 1976). However, we revealed a very short cilium on each ectoderm cell (Figs. 8b, 9n–n″, 9o, o′). These cilia are reminiscent of rudimentary cilia, emerging either transiently during cell differentiation (Boelsterli 1977) or remaining as a rudiment in differentiated cells (Gardiner and Rieger 1980; Rieger and Lombardi 1987). Obviously, they cannot function as a propelling tool, since they even do not have an upright position and their number is ridiculously small; nevertheless, we cannot exclude that they do have certain role in planula life.

Staurozoan larvae were known to develop cnidocytes at the posterior third of the body in a few days after hatching (Kowalevsky 1884; Wietrzykowski 1912). Our ultrastructural analysis reveals that differentiation of capsules begins earlier, right after hatching (Fig. 8a, d, e). Moreover, we assume that the commitment of these cells to cnidocyte pathway occurs much earlier, at the beginning of AP axis differentiation: it is likely, that rounded basiepithelial cells (Figs. 5, 6, 7, 10) are in fact cnidoblasts at an early stage of differentiation. Though they do not have morphological characteristics (capsule, thread) of a cnidoblast, their shape, size, and location are very similar to those of cnidoblasts of planulae.

Evolutionary trend towards a reduction in number of cells in early development: bypassing constraints

Our study showed that early development of *Lucernaria* is very similar to that of other staurozoans (*Lucernaria campanulate* (=*Calvadosia campanulata*), *Halyclistus*

stejnegeri, *Halyclistus salpinx*, *Halyclistus octoradius*, and *Thaumatoscyphus distinctus* (=*Manania uchidai*)) (Bergh 1888; Hanaoka 1934; Kowalevsky 1884; Miranda et al. 2018; Otto 1976; Wietrzykowski 1910, 1912). So, it is implausible that these ontogenies evolved independently. Since these species belong to both suborders of Staurozoa, Myostaurida and Amyostaurida (Miranda et al. 2016, 2018), we hypothesize that the trend towards the reduction of cell number in early development emerged very early in staurozoan evolution.

It is important to note that embryos of many other cnidarian species consist of much higher number of cells than the staurozoan ones. In the hydrozoan *Hydractinia*, gastrulation by delamination starts at the 32-cell stage, but mid-gastrula stage embryos already consist of about 2000 cells (Kraus et al. 2014; Plickert et al. 1988). The hydrozoan *Clytia* gastrulates by unipolar ingression, and embryos have approximately 800 cells in the very beginning of gastrulation (according to images from Kraus et al. 2020). The similar number of cells (700–1000) were found in early gastrula stage embryos of the scyphozoan *Aurelia* (Yuan et al. 2008). What exact constraints do the embryos evolving towards low cell number face? A depleted set of morphogenetic processes as we have seen in *Lucernaria* (Fig. 12a–e). If we analyze the set of morphogenetic movements available for medusozoan cnidarians (Hydrozoa, Scyphozoa, and Staurozoa) (Fig. 12), we find that some developmental trajectories are not accessible for staurozoans by default, as they are based on the coherent behavior of *multiple* cells. These trajectories are based on invagination (Fig. 12a, h, j, k), which is characteristic for scyphozoans, and on the ingression of multiple cells (Fig. 12a, h, i, k), which is very typical for hydrozoans (Berrill 1949; Byrum 2001; Kraus et al. 2020; Metschnikoff 1886). Some other trajectories, e.g., primary and secondary delamination (Fig. 12a, f, g, k and a, h, g, k), occurring in hydrozoan embryos (Kraus and Markov 2017; van de Vyver 1964), were not realized in staurozoan evolution. If we assume that the staurozoan's common ancestor gastrulated by invagination, then the reason for this absence is, perhaps, evolutionary history of the group (so-called phylogenetic inertia) since ingression, unlike delamination, is easily derived from invagination (van der Sande et al. 2020). We can only speculate that transitions to high number of cells during cleavage (Fig. 12h) or gastrula stages (Fig. 12g) are constrained by the natural selection favoring the reduction of cell number in staurozoan embryos.

Staurozoans are not unique in having few cells in embryos. There is a wide range of groups such as Nematoda, Rotifera, Gastrotricha, Sipunculida, Gastropoda, and Tunicata, some representatives of which have small number of cells in their embryos. Nonetheless, they all end up developing phylum-specific bauplans (Hejnol 2010; Schierenberg 2001; Schulze and Schierenberg 2011). This means that these animals successfully bypass the constraints imposed by the number of cells using very peculiar developmental trajectories.

What is so peculiar in developmental trajectories of the animals having very few cells in embryos? Remarkably, early embryos of *Lucernaria* and the aforementioned animals from very distant phylogenetic groups look very similar. Their blastula lacks (or almost lacks) blastocoel and consists of 16–64

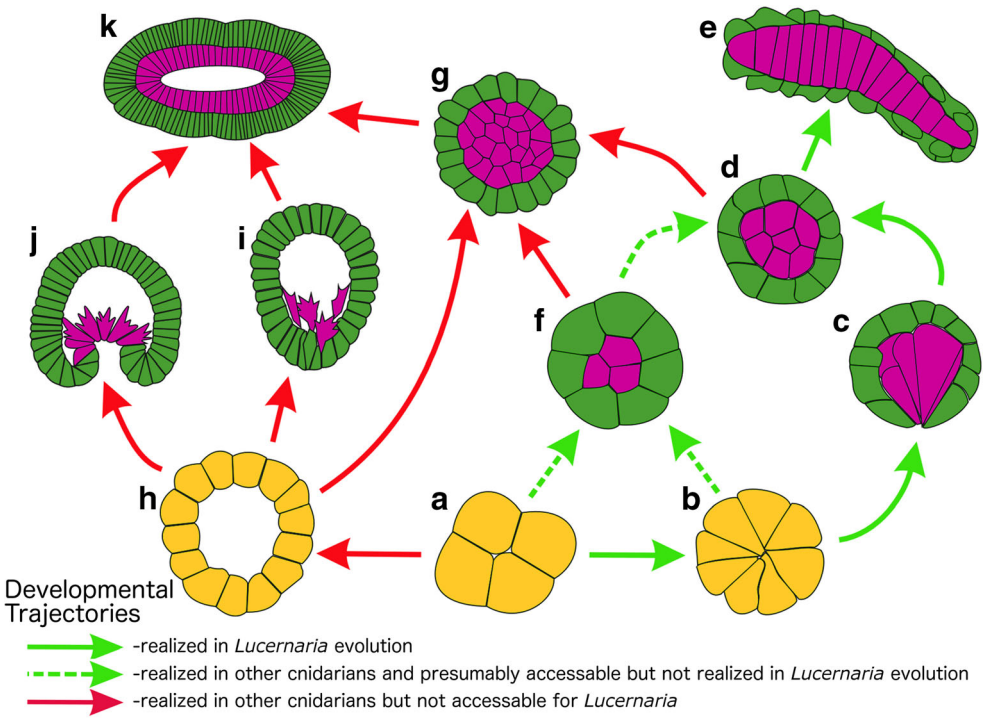

Fig. 12 The set of developmental pathways available for medusozoan cnidarians. Blastomeres are yellow, ectoderm cells are green, and endoderm cells are purple. (**a–e**) Developmental trajectory of *Lucernaria*. (**a**) Cleavage, (**b**) stereoblastula, (**c**) gastrulation by ingression of just a few cells, (**d**) gastrula, (**e**) planula. (**f, g** and **h–k**) Developmental trajectories of other medusozoan cnidarians leading to development of multicellular planula (**k**). (**f**) Gastrulation by primary (cellular) delamination followed by proliferation of both ectoderm and endoderm cells (**g**). (**h**) Blastula containing multiple cells and having the blastocoel (coeloblastula). (**i**) Gastrulation by ingression of multiple cells. (**j**) Gastrulation by invagination

blastomeres, blastomeres are large in relation to the size of an embryo, vegetal cells are often (but not always!) bigger than animal ones. It is not surprising that morphogenetic movements during gastrulation in these animals look the same: presumptive endoderm, which consists of very few cells (e.g., only 2 cells in nematodes and gastrotrichs) undergoes very peculiar type of ingression that was called "dense ingression" (Ivanova-Kazas 1995). During dense ingression, presumptive endoderm cells do not ingress and crawl inside the embryo one by one to fill the blastocoel. Instead, they redistribute cell contents and detach apices, and this is enough to bring these cells to their final position. Dense ingression is always followed by epiboly of ectoderm cells (Ivanova-Kazas 1995).

Indeed, the mode of gastrulation strongly depends on the number of cells. The tunicate appendicularians have 32-cell blastula and gastrulate by ingression followed by epiboly (Fujii et al. 2008). However, 76–110 cells seem to be enough for the embryos to gastrulate by invagination that is observed in other tunicates, specifically ascidians (Jeffery 1992; Nishida 1986). Likewise, the low cell number embryos of nematodes gastrulate by ingression (Schierenberg 2006; Sulston et al. 1983), while nematodes with higher number of cells gastrulate by invagination (Schulze and Schierenberg 2011).

Therefore, in the embryos with low number of cells, cell reshaping substitutes actual cell movements. This we observe not only in gastrulation but also in the process of cell intercalation occurring during endoderm rod formation in *Lucernaria* or during dorsal epidermal intercalation in *C. elegans* (Chin-Sang and Chisholm 2000). It seems that epithelial sheet morphogeneses (such as epithelial folding) are rarely employed in the development of low cell number embryos. For instance, appendicularian neurulation does not rely on the folding of neural plate (Fujii et al. 2008).

Another constraint, which could affect the development of animals evolving towards the reduction of cell number in embryos and larvae, is a low threshold of mechanical instability that could decrease developmental robustness. In the embryos with high number of cells (such as amphibians), changes in the shape and mechanical state of individual cells add up to mechanical state and reshaping of tissues only if they occur in multiple cells at once. As we described for *Lucernaria*, each individual cell constitutes so large a part of an embryo or larva, that reshaping of any cell immediately leads to changes in the mechanical state of the whole organism and may trigger dramatic developmental consequences. We can find very similar situation in ascidians, where the blastopore lip consists (on sections) of only one cell, which does almost the same job as the multicellular blastopore lip in vertebrate embryos (Sherrard et al. 2010).

Therefore, low cell number embryos "had to learn" how to provide developmental robustness under an increased morphogenetic role of each individual embryonic cell.

It was inferred that in few cell embryos of Nematoda, Spiralia, and Chordata developmental trajectories include, but are not limited to, determinant rather than regulative developmental mode; early establishment of cell linages; high importance of maternal transcriptional factors; fast life cycle (Hejnol 2010; Holland 2014; Lambert 2010; Schulze and Schierenberg 2011). A reduced role of regulative genes in early development is reflected in that the genes are clustered in operons in both nematodes and ascidians (Blumenthal et al. 2005; Denoeud et al. 2010; Paps et al. 2012; Pettitt et al. 2014; Satou et al. 2008; Tsagkogeorga et al. 2012). Moreover, many *Hox* genes were lost in nematodes (Aboobaker and Blaxter 2010) and tunicates (Ikuta and Saiga 2005; Seo et al. 2004). It will be interesting to find out if staurozoans follow these trends and to what extent, especially taking into account that early establishment of cell linages and mosaic development are not typical for cnidarians in general.

The much more challenging question is why the animals would reprogram their development for reduction of cell number in embryos. One possible explanation is that this might be the way to accelerate early development: the embryo does not waste time and energy on multiple cell divisions and starts gastrulating when it contains just a few dozen cells. By acceleration of early development animals might benefit from the temporal reduction of the stage of vulnerable, defenseless, and non-feeding embryo (Strathmann et al. 2002) or from favorable conditions in ecologically unstable biotopes (Schierenberg 2001). On the other hand, reduction of cell number can be considered as a side-effect of a positive selection for the higher fecundity, that is typical for sedentary animals or animals facing unstable environment. Production of minute size eggs enables the increased number of offspring (Carrière and Roff 1995; Rosenheim 1996). Since there are certain limits in cell size diminution (Polilov 2015, 2016), the decrease of embryo size from a certain point could be reached by decrease of blastomere number only, not blastomere size. However, reduction of cell number does not always correlate with small size of an egg. For example, in spiralians, low number of cells at the gastrula stage is a characteristic feature of species with relatively big yolky eggs (Hejnol 2010; Ivanova-Kazas 1995).

We can only speculate on the scenario of *Lucernaria* ontogeny evolution, but there is an obvious causal connection between evolutionary changes in the number of embryonic cells and in the life cycle and reproductive strategy.

Taken together, we described and analyzed the dynamics of cell shape changes during early development of the staurozoan *Lucernaria*. From our data, we inferred how the embryo overcomes the constraints imposed by the low number of cells by using very peculiar developmental trajectory. We reconstructed the morphogenetic bases of this trajectory and suggested a link between morphogenetic movements and mechanical stresses orchestrating the development of a few

cell embryo. This is the first step in our understanding of the development of these fascinating animals; the next steps will require unraveling molecular basis of morphogenetic events described here. Moreover, little is known about metamorphosis in staurozoans: there are no convincing data on the morphogenesis of a primary polyp, which is another mystery of this unique group.

Acknowledgments We thank N.A. Pertsov White Sea Biological Station of Moscow State University for the help and support in obtaining samples and providing access to all required facilities and equipment of the "Center of Microscopy WSBS MSU". We are very grateful to the Shared Facilities center "Electron Microscopy for Life Sciences" of the Lomonosov Moscow State University for the possibility to perform TEM. We want to express special gratitude to Catriona Munro (Collège de France, Center for Interdisciplinary Research in Biology) and members of the Villefranche-sur-mer Developmental Biology Laboratory for manuscript critical reading and advice. The authors thank Brigit Shea Sullivan, NIH Library Editing Service, for manuscript editing assistance.

Authors' contributions Y.K. and T.M. designed the research; T.M., B.O., and Y.K. performed the in vivo and TEM studies; T.M. and Y.K. performed confocal microscopy; T.M. and Y.K. analyzed the data and wrote the paper.

Funding This study was funded by the Russian Foundation for Basic Research (grant # 15-04-08214-a) and by the Governmental Basic Research Program for the Koltzov Institute of Developmental Biology of the Russian Academy of Sciences (0108-2019-0003).

Data Availability all data generated or analyzed during this study are included in this published article; original images generated in the course of light, confocal, and electron microscopy studies are available by request.

Compliance with ethical standards

Conflict of interest The authors declare that they have no conflict of interest.

Ethics approval Not applicable.

Consent to participate Not applicable.

Consent for publication Not applicable.

Code availability Not applicable.

References

Aboobaker, A., & Blaxter, M. (2010). The nematode story: Hox gene loss and rapid evolution. In J. S. Deutsch (Ed.), *Hox genes. Advances in experimental medicine and biology* (pp. 101–110). Springer. https://doi.org/10.1007/978-1-4419-6673-5_7.

Adams, D. S., Keller, R., & Koehl, M. A. (1990). The mechanics of notochord elongation, straightening and stiffening in the embryo of Xenopus laevis. *Development (Cambridge, England), 110*(1), 115–130. https://doi.org/10.1093/icb/40.1.53.

Beloussov, L. V. (1996). Patterns of mechanical stresses and formation of the body plans in animal embryos. *Verhandlungen der Deutschen Zoologischen Gesellschaft, 89*, 219–229.

Bergh, R. S. (1888). Bemaerkninger om Udviklingen af Lucernaria. *Vidensk Meddel Naturhist Foren Kjøbenhavn, 1888*, 214–220.

Berrill, N. J. (1949). Developmental analysis of Scyphomedusae. *Biological Reviews, 24*(4), 393–409. https://doi.org/10.1111/j.1469-185X.1949.tb00581.x.

Blankenship, J. T., Backovic, S. T., Sanny, J. S. P., Weitz, O., & Zallen, J. A. (2006). Multicellular rosette formation links planar cell polarity to tissue morphogenesis. *Developmental Cell, 11*(4), 459–470. https://doi.org/10.1016/j.devcel.2006.09.007.

Blumenthal, T., Davis, P., & Garrido-Lecca, A. (2005). Operon and non-operon gene clusters in the C. elegans genome. In *WormBook*. https://doi.org/10.1895/wormbook.1.175.1.

Boelsterli, U. (1977). An electron microscopic study of early developmental stages, myogenesis, oogenesis and cnidogenesis in the anthomedusa, Podocoryne carnea M. Sars. *Journal of Morphology, 154*(2), 259–289. https://doi.org/10.1002/jmor.1051540206.

Boero, F., Bouillon, J., & Piraino, S. (1992). On the origins and evolution of hydromedusan life cycles (Cnidaria, Hydrozoa). *Sex Origin and Evolution, 6*, 59–68.

Burggren, W. W., & Reyna, K. S. (2011). Developmental trajectories, critical windows and phenotypic alteration during cardio-respiratory development. *Respiratory Physiology & Neurobiology, 178*(1), 13–21. https://doi.org/10.1016/j.resp.2011.05.001.

Burmistrova, Y. A., Osadchenko, B. V., Bolshakov, F. V., Kraus, Y. A., & Kosevich, I. A. (2018). Embryonic development of thecate hydrozoan Gonothyraea loveni (Allman, 1859). *Development, Growth & Differentiation, 60*(8), 483–501. https://doi.org/10.1111/dgd.12567.

Byrum, C. A. (2001). An analysis of hydrozoan gastrulation by unipolar ingression. *Developmental Biology, 240*(2), 627–640. https://doi.org/10.1006/dbio.2001.0484.

Carrière, Y., & Roff, D. A. (1995). The evolution of offspring size and number: a test of the Smith-Fretwell model in three species of crickets. *Oecologia, 102*(3), 389–396. https://doi.org/10.1007/BF00329806.

Chin-Sang, I. D., & Chisholm, A. D. (2000). Form of the worm: genetics of epidermal morphogenesis in C. elegans. *Trends in Genetics, 16*(12), 544–551. https://doi.org/10.1016/S0168-9525(00)02143-0.

Clark, A. G., Wartlick, O., Salbreux, G., & Paluch, E. K. (2014). Stresses at the cell surface during animal cell morphogenesis. *Current Biology, 24*(10), R484–R494. https://doi.org/10.1016/j.cub.2014.03.059.

Clark, E. (2017). Dynamic patterning by the Drosophila pair-rule network reconciles long-germ and short-germ segmentation. *PLoS Biology, 15*(9), e2002439. https://doi.org/10.1371/journal.pbio.2002439.

Collins, A., Schuchert, P., Marques, A., Jankowski, T., Medina, M., & Schierwater, B. (2006). Medusozoan phylogeny and character evolution clarified by new large and small subunit rDNA data and an assessment of the utility of phylogenetic mixture models. *Systematic Biology, 55*(1), 97–115. https://doi.org/10.1080/10635150500433615.

Denoeud, F., Henriet, S., Mungpakdee, S., Aury, J. M., Da Silva, C., Brinkmann, H., Mikhaleva, J., Olsen, L. C., Jubin, C., Cañestro, C., Bouquet, J. M., Danks, G., Poulain, J., Campsteijn, C., Adamski, M., Cross, I., Yadetie, F., Muffato, M., Louis, A., et al. (2010). Plasticity of animal genome architecture unmasked by rapid evolution of a pelagic tunicate. *Science, 330*(6009), 1381–1385. https://doi.org/10.1126/science.1194167.

Fujii, S., Nishio, T., & Nishida, H. (2008). Cleavage pattern, gastrulation, and neurulation in the appendicularian, Oikopleura dioica. *Development Genes and Evolution, 218*(1–2), 69–79. https://doi.org/10.1007/s00427-008-0205-4.

Gardiner, S. L., & Rieger, R. M. (1980). Rudimentary cilia in muscle cells of annelids and echinoderms. *Cell and Tissue Research, 213*(2), 247–252. https://doi.org/10.1007/BF00234785.

Gudipaty, S. A., Lindblom, J., Loftus, P. D., Redd, M. J., Edes, K., Davey, C. F., Krishnegowda, V., & Rosenblatt, J. (2017). Mechanical stretch triggers rapid epithelial cell division through Piezo1. *Nature, 543*(7643), 118–121. https://doi.org/10.1038/nature21407.

Haas, P. A., Höhn, S. S. M. H., Honerkamp-Smith, A. R., Kirkegaard, J. B., & Goldstein, R. E. (2018). The noisy basis of morphogenesis: mechanisms and mechanics of cell sheet folding inferred from developmental variability. *PLoS Biology, 16*(7), e2005536. https://doi.org/10.1371/journal.pbio.2005536.

Hanaoka, K.-I. (1934). Notes on the early development of a stalked medusa. In *Proceedings of the Imperial Academy* (Vol. 10, pp. 117–120). https://doi.org/10.2183/pjab1912.10.117.

Hejnol, A. (2010). A twist in time-the evolution of spiral cleavage in the light of animal phylogeny. *Integrative and Comparative Biology, 50*(5), 695–706. https://doi.org/10.1093/icb/icq103.

Holland, L. Z. (2014). Genomics, evolution and development of amphioxus and tunicates: the Goldilocks principle. *Journal of Experimental Zoology Part B: Molecular and Developmental Evolution, 324*(4), 342–352. https://doi.org/10.1002/jez.b.22569.

Ikuta, T., & Saiga, H. (2005). Organization of Hox genes in ascidians: present, past, and future. *Developmental Dynamics, 233*(2), 382–389. https://doi.org/10.1002/dvdy.20374.

Ivanova-Kazas, O. M. (1995). Evolutionary embryology of animals. In *Evolutionary embryology of animals.* St. Petersburg, Nauka.

Jeffery, W. R. (1992). A gastrulation center in the ascidian egg. *Development, 116*(S), 53–63.

Kalinka, A. T., & Tomancak, P. (2012). The evolution of early animal embryos: conservation or divergence? *Trends in Ecology & Evolution, 27*(7), 385–393. https://doi.org/10.1016/j.tree.2012.03.007.

Keller, R., Davidson, L., Edlund, A., Elul, T., Ezin, M., Shook, D., & Skoglund, P. (2000). Mechanisms of convergence and extension by cell intercalation. *Philosophical Transactions of the Royal Society, B: Biological Sciences, 355*(1399), 897–922. https://doi.org/10.1098/rstb.2000.0626.

Kowalevsky, A. (1884). Zur Entwicklungsgeschichte der Lucernaria. *Zoologischer Anzeiger, 7*, 712–717.

Kraus, Y. A. (2006). Morphomechanical programming of morphogenesis in Cnidarian embryos. *International Journal of Developmental Biology, 50*(2–3), 267–275. https://doi.org/10.1387/ijdb.052061yk.

Kraus, Y., Chevalier, S., & Houliston, E. (2020). Cell shape changes during larval body plan development in Clytia hemisphaerica. *Developmental Biology, 468*(1–2), 59–79. https://doi.org/10.1016/j.ydbio.2020.09.013.

Kraus, Y. A., Flici, H., Hensel, K., Plickert, G., Leitz, T., & Frank, U. (2014). The embryonic development of the cnidarian Hydractinia echinata. *Evolution and Development, 16*(6), 323–338. https://doi.org/10.1111/ede.12100.

Kraus, Y. A., & Markov, A. V. (2017). The gastrulation in Cnidaria: a key to understanding phylogeny or the chaos of secondary modifications? *Biology Bulletin Reviews, 7*(1), 7–25. https://doi.org/10.1134/s2079086417010029.

Kraus, Y. A., & Technau, U. (2006). Gastrulation in the sea anemone Nematostella vectensis occurs by invagination and immigration: an ultrastructural study. *Development Genes and Evolution, 216*(3), 119–132. https://doi.org/10.1007/s00427-005-0038-3.

Lambert, J. D. (2010). Developmental patterns in spiralian embryos. *Current Biology, 20*(2), R72–R77. https://doi.org/10.1016/j.cub.2009.11.041.

Leclère, L., Copley, R. R., Momose, T., & Houliston, E. (2016). Hydrozoan insights in animal development and evolution. *Current Opinion in Genetics and Development, 39*, 157–167. https://doi.org/10.1016/j.gde.2016.07.006.

Lecuit, T., & Lenne, P. F. (2007). Cell surface mechanics and the control of cell shape, tissue patterns and morphogenesis. *Nature Reviews Molecular Cell Biology, 8*(8), 633–644. https://doi.org/10.1038/nrm2222.

Liu, M., Xu, J., Tanswell, A. K., & Post, M. (1993). Stretch-induced growth-promoting activities stimulate fetal rat lung epithelial cell proliferation. *Experimental Lung Research, 19*, 505–517.

Lynch, J. A., El-Sherif, E., & Brown, S. J. (2012). Comparisons of the embryonic development of Drosophila, Nasonia, and Tribolium. *Wiley Interdisciplinary Reviews: Developmental Biology, 1*(1), 16–39. https://doi.org/10.1002/wdev.3.

Metschnikoff, E. (1886). Embryologische Studien an Medusen. In A. Holder & E. Metschnikoff (Eds.), *Ein Beitrag zur Genealogie der Primitiv-organe*. https://doi.org/10.5962/bhl.title.5982.

Miranda, L. S., Hirano, Y. M., Mills, C. E., Falconer, A., Fenwick, D., Marques, A. C., & Collins, A. G. (2016). Systematics of stalked jellyfishes (Cnidaria: Staurozoa). *PeerJ, 4*, e1951. https://doi.org/10.7717/peerj.1951.

Miranda, L. S., Mills, C. E., Hirano, Y. M., Collins, A. G., & Marques, A. C. (2018). A review of the global diversity and natural history of stalked jellyfishes (Cnidaria, Staurozoa). *Marine Biodiversity, 48*, 1695–1714. https://doi.org/10.1007/s12526-017-0721-4.

Momose, T., & Schmid, V. (2006). Animal pole determinants define oral-aboral axis polarity and endodermal cell-fate in hydrozoan jellyfish Podocoryne carnea. *Developmental Biology, 292*(2), 371–380. https://doi.org/10.1016/j.ydbio.2006.01.012.

Nishida, H. (1986). Cell division pattern during gastrulation of the ascidian, Halocynthia roretzi (cell division pattern/gastrulation/neurulation/ascidian embryo). *Development, Growth & Differentiation, 28*(2), 191–201. https://doi.org/10.1111/j.1440-169X.1986.00191.x.

Otto, J. J. (1976). Early development and planula movement in Haliclystus (Scyphozoa: Stauromedusae). In G. O. Mackie (Ed.), *Coelenterate ecology and behavior* (pp. 319–329). Springer. https://doi.org/10.1007/978-1-4757-9724-4_34.

Paps, J., Holland, P. W. H., & Shimeld, S. M. (2012). A genome-wide view of transcription factor gene diversity in chordate evolution: less gene loss in amphioxus? *Briefings in Functional Genomics, 11*(2), 177–186. https://doi.org/10.1093/bfgp/els012.

Pettitt, J., Philippe, L., Sarkar, D., Johnston, C., Gothe, H. J., Massie, D., Connolly, B., & Müller, B. (2014). Operons are a conserved feature of nematode genomes. *Genetics, 197*(4), 1201–1211. https://doi.org/10.1534/genetics.114.162875.

Plickert, G., Kroiher, M., & Munck, A. (1988). Cell proliferation and early differentiation during embryonic development and metamorphosis of Hydractinia echinata. *Development, 103*(4), 795–803.

Polilov, A. A. (2015). Small is beautiful: features of the smallest insects and limits to miniaturization. *Annual Review of Entomology, 60*, 103–121. https://doi.org/10.1146/annurev-ento-010814-020924.

Polilov, A. A. (2016). At the size limit-effects of miniaturization in insects. In *At the size limit-effects of miniaturization in insects*. Springer. https://doi.org/10.1007/978-3-319-39499-2.

Priess, J., & Hirsh, D. I. (1986). Caenorhabditis elegans morphogenesis: the role of the cytoskeleton in elongation of the embryo. *Developmental Biology, 117*(1), 156–173. https://doi.org/10.1016/0012-1606(86)90358-1.

Raff, R. A. (1992). Evolution of developmental decisions and morphogenesis: the view from two camps. *Development, 116*(S), 15–22.

Raikova, E. V. (1990). Fine structure of the nematocytes of Polypodium hydriforme Ussov (Cnidaria). *Zoologica Scripta, 19*(1), 1–11. https://doi.org/10.1111/j.1463-6409.1990.tb00236.x.

Rieger, R. M., & Lombardi, J. (1987). Ultrastructure of coelomic lining in echinoderm podia: significance for concepts in the evolution of muscle and peritoneal cells. *Zoomorphology, 107*(4), 191–208. https://doi.org/10.1007/BF00312261.

Rifkin, J. F., & Endean, R. (1988). Arrangement of accessory cells and nematocytes bearing mastigophores in the tentacles of the cubozoan Chironex fleckeri. *Journal of Morphology, 195*(1), 103–115. https://doi.org/10.1002/jmor.1051950110.

Roh-Johnson, M., Shemer, G., Higgins, C. D., McClellan, J. H., Werts, A. D., Tulu, U. S., Gao, L., Betzig, E., Kiehart, D. P., & Goldstein, B. (2012). Triggering a cell shape change by exploiting preexisting actomyosin contractions. *Science, 335*(6073), 1232–1235. https://doi.org/10.1126/science.1217869.

Rosenheim, J. A. (1996). An evolutionary argument for egg limitation. *Evolution, 50*(5), 2089–2094. https://doi.org/10.1111/j.1558-5646.1996.tb03595.x.

Salbreux, G., Charras, G., & Paluch, E. (2012). Actin cortex mechanics and cellular morphogenesis. *Trends in Cell Biology, 22*(10), 536–545. https://doi.org/10.1016/j.tcb.2012.07.001.

Satou, Y., Mineta, K., Ogasawara, M., Sasakura, Y., Shoguchi, E., Ueno, K., Yamada, L., Matsumoto, J., Wasserscheid, J., Dewar, K., Wiley, G. B., Macmil, S. L., Roe, B. A., Zeller, R. W., Hastings, K. E. M., Lemaire, P., Lindquist, E., Endo, T., Hotta, K., & Inaba, K. (2008). Improved genome assembly and evidence-based global gene model set for the chordate Ciona intestinalis: new insight into intron and operon populations. *Genome Biology, 9*(10), R152. https://doi.org/10.1186/gb-2008-9-10-r152.

Sawyer, J. M., Harrell, J. R., Shemer, G., Sullivan-Brown, J., Roh-Johnson, M., & Goldstein, B. (2010). Apical constriction: a cell shape change that can drive morphogenesis. *Developmental Biology, 341*(1), 5–19. https://doi.org/10.1016/j.ydbio.2009.09.009.

Schierenberg, E. (2001). Three sons of fortune: early embryogenesis, evolution and ecology of nematodes. *BioEssays, 23*(9), 841–847. https://doi.org/10.1002/bies.1119.

Schierenberg, E. (2006). Embryological variation during nematode development. In J. Priess & G. Seydoux (Eds.), *WormBook*. https://doi.org/10.1895/wormbook.1.55.1.

Schulze, J., & Schierenberg, E. (2011). Evolution of embryonic development in nematodes. *EvoDevo, 2*(1), 18. https://doi.org/10.1186/2041-9139-2-18.

Seo, H. C., Edvardsen, R. B., Maeland, A. D., Bjordal, M., Jensen, M. F., Hansen, A., Flaat, M., Weissenbach, J., Lehrach, H., Reinhardt, R., & Chourrout, D. (2004). Hox cluster disintegration with persistent anteroposterior order of expression in Oikopleura dioica. *Nature, 431*, 67–71. https://doi.org/10.1038/nature02709.

Sherrard, K., Robin, F., Lemaire, P., & Munro, E. (2010). Sequential activation of apical and basolateral contractility drives ascidian endoderm invagination. *Current Biology, 20*(17), 1499–1510. https://doi.org/10.1016/j.cub.2010.06.075.

Shook, D. R., Kasprowicz, E. M., Davidson, L. A., & Keller, R. (2018). Large, long range tensile forces drive convergence during Xenopus blastopore closure and body axis elongation. *ELife, 7*, e26944. https://doi.org/10.7554/eLife.26944.

Shook, D. R., & Keller, R. (2003). Mechanisms, mechanics and function of epithelial-mesenchymal transitions in early development. *Mechanisms of Development, 120*(11), 1351–1383. https://doi.org/10.1016/j.mod.2003.06.005.

Shook, D. R., & Keller, R. (2008). Morphogenic machines evolve more rapidly than the signals that pattern them: lessons from amphibians. *Journal of Experimental Zoology Part B: Molecular and Developmental Evolution, 310*(1), 111–135. https://doi.org/10.1002/jez.b.21204.

Simske, J. S., & Hardin, J. (2001). Getting into shape: epidermal morphogenesis in Caenorhabditis elegans embryos. *BioEssays, 23*(1), 12–23. https://doi.org/10.1002/1521-1878(200101)23:1<12::AID-BIES1003>3.0.CO;2-R.

Smith, F. J., Percival, C. J., Young, N. M., Hu, D., Schneider, R. A., Marcucio, R. S., & Hallgrimsson, B. (2015). Divergence of craniofacial developmental trajectories among avian embryos. *Developmental Dynamics, 244*(9), 1158–1167. https://doi.org/10.1002/dvdy.24262.

Strathmann, R. R., Staver, J. M., & Hoffman, J. R. (2002). Risk and the evolution of cell-cycle durations of embryos. *Evolution, 56*(4), 708–720. https://doi.org/10.1111/j.0014-3820.2002.tb01382.x.

Sulston, J. E., Schierenberg, E., White, J. G., & Thomson, J. N. (1983). The embryonic cell lineage of the nematode Caenorhabditis elegans. *Developmental Biology, 100*(1), 64–119. https://doi.org/10.1016/0012-1606(83)90201-4.

Thomas, K. A., & Stemple, D. L. (2004). Development of the zebrafish organizer and notochord. In Z. Gong & V. Korzh (Eds.), *Fish development and genetics* (pp. 87–120). World Scientific. https://doi.org/10.1142/9789812565761_0003.

Tsagkogeorga, G., Cahais, V., & Galtier, N. (2012). The population genomics of a fast evolver: high levels of diversity, functional constraint, and molecular adaptation in the tunicate Ciona intestinalis. *Genome Biology and Evolution, 4*(8), 852–861. https://doi.org/10.1093/gbe/evs054.

van der Sande, M., Kraus, Y. A., Houliston, E., & Kaandorp, J. (2020). A cell-based boundary model of gastrulation by unipolar ingression in the hydrozoan cnidarian Clytia hemisphaerica. *Developmental Biology, 460*(2), 176–186. https://doi.org/10.1016/j.ydbio.2019.12.012.

van de Vyver, G. (1964). Etude histologique du developpement d'Hydractinia echinata. *Cahiers de Biologie Marine, 5*, 295–310.

Westfall, J. A. (1966). The differentiation of nematocysts and associated structures in the cnidaria. *Zeitschrift für Zellforschung und Mikroskopische Anatomie, 75*(2), 381–403. https://doi.org/10.1007/BF00336871.

Wietrzykowski, W. (1910). Sur le développement des Lucernaridés (note préliminaire). *Archives de Zoologie Expérimentale, 5*, 10–27.

Wietrzykowski, W. (1912). Recherches sur le developpement des Lucernaires. *Archives de Zoologie Expérimentale et Générale, 10*, 1–95.

Wray, G. A., & Raff, R. A. (1991). The evolution of developmental strategy in marine invertebrates. *Trends in Ecology & Evolution, 45*, 1741–1750. https://doi.org/10.1016/0169-5347(91)90121-D.

Yuan, D., Nakanishi, N., Jacobs, D. K., & Hartenstein, V. (2008). Embryonic development and metamorphosis of the scyphozoan Aurelia. *Development Genes and Evolution, 218*(10), 525–539. https://doi.org/10.1007/s00427-008-0254-8.